SIAM J. APPL. MATH.
Vol. 0, No. 0, pp. 000–000

RECONSTRUCTING COMPLEX FLUID PROPERTIES FROM THE BEHAVIOR OF FLUCTUATING IMMERSED PARTICLES*

CHRISTEL HOHENEGGER† AND SCOTT A. MCKINLEY‡

Abstract. Complex fluids have long been characterized by two functions that summarize the fluid's elastic and viscous properties, respectively called the storage ($G'(\omega)$) and loss ($G''(\omega)$) moduli. A fundamental observation in this field, which is called *passive microrheology*, is that information about these bulk fluid properties can be inferred from the path statistics of immersed, fluctuating microparticles. In this work, we perform a systematic study of the multistep protocol that forms the foundation of this field. Particle velocities are assumed to be well described by the Generalized Langevin Equation, a stochastic integro-differential equation uniquely characterized by a memory kernel $G_r(t)$, which is hypothesized to be inherited from the surrounding fluid. We investigate the covariation between a particle's velocity process and the non-Markovian fluctuations that force it, and we establish rigorous justification for a key relationship between a particle's Mean Squared Displacement and its memory kernel $G_r(t)$. With this foundation in hand, by way of a tunable four-parameter family of functions that can serve as particle memory functions, we analyze errors and uncertainties intrinsic in passive microrheology techniques. We show that, despite the fact that certain parameters are essentially unidentifiable on their own, the protocol is remarkably effective in reconstructing $G'(\omega)$ and $G''(\omega)$ in a range that corresponds to the experimentally observable regime.

Key words. microrheology, generalized Langevin equation, complex fluids, inference

AMS subject classifications. 76A10, 60H10

DOI. 10.1137/17M1131660

1. Introduction.

Rheology is the study of the flow and deformation of soft matter, especially in response to applied forces. For materials ranging from polymer melts to cake batter, the theory of rheology has provided insight and a common language for describing both the fluid-like and solid-like properties of complex fluids [24]. Traditionally, the experiments that assess these properties require liters of material, but this poses a serious problem when investigating biological materials. While there is no problem producing liters to sample for many materials used in industry, this is simply not possible for biological fluids like mucus and cytoplasm. The advent of nano-scale single particle tracking opened the way for new modes of investigation. In their seminal paper, Mason and Weitz [27] were able to relate the statistics of individual particle paths with bulk fluid properties. Over the last 20 years, there have been numerous modifications and extensions to the theory [28, 39, 40, 25, 16, 4], which has become a vital tool for investigating characterizing healthy and unhealthy mucus, blood, and various biofilms [41, 2, 29, 22, 23, 3].

While the theory has been validated in some special cases, it is important to note that most inference protocols involve either (1) numerical computation of Laplace transforms, or (2) fitting of power laws on log-log plots [28, 6]. Both of these methods

*Received by the editors May 25, 2017; accepted for publication (in revised form) May 30, 2018; published electronically DATE.

http://www.siam.org/journals/siap/x-x/M113166.html

Funding: The first author's work was supported by NSF DMS-1412998. The second author's work was supported by NSF DMS-1644290.

†Department of Mathematics, University of Utah, Salt Lake City, UT 84112 (choheneg@math.utah.edu).

‡Department of Mathematics, Tulane University, New Orleans, LA 70118 (scott.mckinley@tulane.edu).

are notoriously noisy and should give us pause to wonder what degree of error they induce. Moreover, while data is collected in the time domain, rheological properties are expressed in frequency space. When experiments are constrained by a camera's frame rate on the one hand, and the tendency to diffuse out of a field of view on the other, it is not immediately clear what the bound of accurate inference will be on the frequency side. These concerns call for a rigorous investigation into the intrinsic uncertainty that arises from the chain of assumptions that constitute a standard microrheological protocol. In this work, we provide such an investigation, demonstrating both strengths and weaknesses that exist in the current paradigm.

1.1. Bulk fluid properties. The linear response of a viscoelastic medium to a shear force is summarized by its shear relaxation modulus $G_r(t)$, which is used to relate a fluid's stress response $\sigma(t)$ to an applied shear rate $\dot\gamma(t)$. A one-dimensional version of such a *constitutive equation* is

$$\sigma(t) = \int_0^t G_r(t-t')\dot\gamma(t')\mathrm{d}t'. \tag{1}$$

It has been experimentally observed that when an oscillatory shear, $\gamma(t) = \gamma_0 \sin(\omega t)$, is applied to a complex fluid, the stress response will also be oscillatory, but possibly out of phase:

$$\begin{aligned}\sigma(t) &= \sigma_0 \sin(\omega t + \phi(\omega)) \\ &= \sigma_0 \cos(\phi(\omega)) \sin(\omega t) + \sigma_0 \sin(\phi(\omega)) \cos(\omega t).\end{aligned} \tag{2}$$

A pure solid will respond in phase, $\phi(t) \equiv 0$, while a viscous fluid will respond out of phase with $\phi(t) \equiv \pi/2$. In general, the phase of the stress response will be ω-dependent. The coefficient of $\sin(\omega t)$ is considered the ω-dependent magnitude of the elastic response, while the coefficient of $\cos(\omega t)$ is the magnitude of the viscous response.

The stress can also be expressed in terms of the shear relaxation modulus $G_r(t)$ and the rate of strain $\dot\gamma(t) = \gamma_0\omega\cos(\omega t)$ through the constitutive equation (1):

$$\begin{aligned}\sigma(t) &= \int_0^t G_r(t-t')\gamma_0\omega\cos(\omega t')\mathrm{d}t' \overset{(u=t-t')}{=} \gamma_0\omega\int_0^t G_r(u)\cos(\omega(t-u))\mathrm{d}u \\ &= \gamma_0\omega\int_0^t G_r(u)\left(\sin(\omega t)\sin(\omega u) + \cos(\omega t)\cos(\omega u)\right)\mathrm{d}u \\ &= \gamma_0\omega\Big(\int_0^t G_r(u)\sin(\omega u)\mathrm{d}u\Big)\sin(\omega t) + \gamma_0\omega\Big(\int_0^t G_r(u)\cos(\omega u)\mathrm{d}u\Big)\cos(\omega t). \qquad (3)\end{aligned}$$

Comparing the coefficients of $\sin(\omega t)$ and $\cos(\omega t)$ in (2) and (3), we see that the elastic and the viscous components of the response can be represented through the Fourier sine and cosine transforms of $G_r(t)$. These are called the *shear storage modulus* $G'(\omega)$ and the *shear loss modulus* $G''(\omega)$, respectively [24]:

$$\begin{aligned}\text{Storage: } G'(\omega) &:= \omega\int_0^\infty G_r(t)\sin(\omega t)\mathrm{d}t, \\ \text{Loss: } G''(\omega) &:= \omega\int_0^\infty G_r(t)\cos(\omega t)\mathrm{d}t.\end{aligned} \tag{4}$$

We note that the use of "primes" in the names G' and G'' is a notational idiom from the rheology literature and does not imply that we are taking derivatives of a function G.

For a purely viscous fluid, the response to shear is instantaneous, so $G_r(t)$ is a Dirac δ-function. In turn, the storage and loss moduli are $G'(\omega) = 0$ and $G''(\omega) = \eta_s\omega$. The relaxation modulus can take on many forms for viscoelastic fluids, but an important class, which we refer to as *generalized Maxwell fluids with intrinsic viscosity*, consists of a Dirac δ-function linearly superimposed with a collection of exponential decay functions called *Maxwell elements*:

$$\text{Viscoelastic Relaxation: } G_r(t) = \eta_s\delta(t) + \sum_{n=1}^{N} G_n e^{-t/\tau_n}\, 1_{\{t\geq 0\}}. \tag{5}$$

The positive values $\{\tau_n\}$ are called *relaxation times*. The values $\{G_n\}$ are also positive and have units of `[stress]`. We use $1_{t\geq 0}$ to denote the unit step function. Throughout this work, we will focus on a special structure, which has been called the *generalized Rouse relaxation spectrum*. See (2.1) for the definition below. The storage and loss moduli are in turn often summarized by the so-called *complex modulus* $G^*(\omega)$, which is defined to be

$$G^*(\omega) := G'(\omega) + iG''(\omega). \tag{6}$$

The complex modulus is related to what is called the *complex viscosity* through the formula $\eta^*(\omega) := G^*(\omega)/i\omega$. By a formal calculation using the definitions of the Fourier transform and of the Fourier sine and cosine transforms, it follows that $\eta^*(\omega) = \widehat{G_r}(\omega)$, where $\hat{\cdot}$ denotes the Fourier transform. As a consequence of the definition (5), we have that $\tilde{\eta}(s) = \widetilde{G_r}(s)$, where $\tilde{\cdot}$ denotes the (unilateral) Laplace transform.

Examples of the shear storage and shear loss moduli for the Generalized Rouse Kernel considered in this work are provided in Figure 1 as a function of the number of Maxwell elements and of its shape parameter ν. The asymptotic behavior near zero is such that $G'(\omega)$ is quadratic (slope 2 on a log-log plot) and $G''(\omega)$ is linear (slope 1 on a log-log plot). For large ω, $G'(\omega)$ is constant, while $G''(\omega)$ grows linearly. The length of the transition region is a function of both the shape parameter and the number of Maxwell elements.

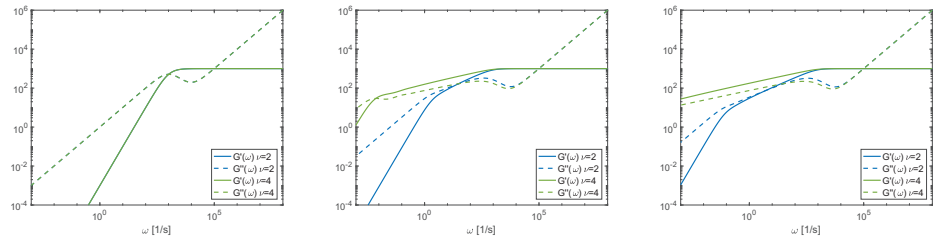

(a) One Maxwell Element (b) 20 Maxwell Elements (c) 100 Maxwell Elements

FIG. 1. Storage and Loss Moduli for Generalized Rouse Kernel *as a function of the number of Maxwell elements. The smallest relaxation time is* $\tau_0 = 10^{-3}$ *s, the solvent viscosity is* $\eta_s = 10^{-2} g/(cm\ s)$*, and the ratio* η_p/τ_{avg} *is the same independently of the number of kernels; here* $\eta_p/\tau_{avg} = 10^3 g/(cm\ s^2)$*. The green curves correspond to a shape parameter* $\nu = 4$*, while the blue curves are obtained with* $\nu = 2$*.*

1.2. Passive microrheology. Let $\big(X(t)\big)_{t\geq 0}$ denote the position of a particle at time t and let $\big(V(t)\big)_{t\geq 0}$ denote its velocity. The classical model for the velocity of

a particle in a viscous fluid is the Langevin Equation:

Langevin Equation

$$m\mathrm{d}V(t) = -\gamma V(t)\mathrm{d}t + \sqrt{2k_BT\gamma}\,\mathrm{d}W(t), \tag{7}$$

where m is the mass of the particle, k_B is Boltzmann constant, T is the temperature of the system, γ is the drag coefficient, and $W(t)$ is a standard Brownian motion. By Stokes Law, if the particle is a sphere of radius a and the fluid has viscosity η_s, then $\gamma = 6\pi a\eta_s$.

Using standard Stochastic Calculus, one can show that

$$\lim_{t\to\infty} \frac{1}{t}\,\mathbb{E}\big(|X(t)|^2\big) = \frac{dk_BT}{3\pi a\eta_s}, \tag{8}$$

where d is the number of observed dimensions. This establishes the fundamental Stokes–Einstein relationship between the viscosity of a fluid and the Mean Squared Displacement (MSD), $M(t) := \mathbb{E}\big(|X(t)|^2\big)$, of an immersed particle.

Intrinsic in the development of the Langevin Equation is the assumption that the diffusing particle of interest is much larger than the particles in the fluid environment that collide with it generating both drag and thermal excitation. For this reason, the Generalized Langevin Equation (GLE) was introduced by Mori [32] and Kubo [20, 19], and soon thereafter Zwanzig and Bixon [44] proposed that the Stokes–Einstein relationship could be generalized for simple viscoelastic fluids. It would be another 25 years, though, before a fully realized connection between viscoelastic diffusion and the GLE was proposed. In their seminal work, Mason and Weitz [27] hypothesized that the drag force experienced by a particle immersed in a viscoelastic fluid is directly proportional to the shear relaxation modulus $G_r(t)$:

Generalized Langevin Equation (Informal Definition)

$$m\dot{V}(t) = -6\pi a\int_{-\infty}^{t} G_r(t-s)V(s)\mathrm{d}s + F(t), \tag{9}$$

where $F(t)$ is a mean-zero, stationary, Gaussian process with an autocovariance function defined so that the velocity process satisfies the equipartition theorem [38]

$$m\mathbb{E}\big(|V(0)|^2\big) = dk_BT. \tag{10}$$

If $G_r(t)$ is purely viscous, i.e., $G_r(t) = \eta_s\delta(t)$, then we recover the Langevin Equation. The convolution term in (9) has been subsequently investigated and justified in [42].

By way of a formal argument using Laplace transforms, Mason and Weitz were the first to establish a relationship between the Laplace transform of a fluid's relaxation modulus $\widetilde{G}_r(s)$ and that of an immersed particle's MSD. In practice, MSD is computed path-by-path by using a within-path sliding average of the covariance at different lag times. Assuming that the jth particle has been observed for N steps uniformly separated by time intervals of length δ, we define the *pathwise MSD* to be

$$\mathcal{M}_j(n\delta) := \frac{1}{N-n+1}\sum_{k=0}^{N-n}\big|X_j\big((n+k)\delta\big) - X_j\big(k\delta\big)\big|^2. \tag{11}$$

When there is no subscript denoting the particle index, we are referring to the ensemble average of J distinct particle paths. We define the *ensemble MSD* to be

$$\mathcal{M}(t) := \frac{1}{J}\sum_{j=1}^{J}\mathcal{M}_j(t), \text{ where } t \in \{0, \delta, 2\delta, \ldots, N\delta\}. \tag{12}$$

We assume linear interpolation for all other t.

This completes the chain of connections that form the basis for passive microrheology, which we summarize as follows:

Passive Microrheology

$$\mathcal{M}(t) \longleftrightarrow M(t) \overset{GLE}{\longleftrightarrow} \widetilde{G}_r(s) \longleftrightarrow (G'(\omega), G''(\omega)). \tag{13}$$

There are multiple proposals for how to approximate and/or efficiently compute each of the $\longleftrightarrow$ connections, each introducing another layer of uncertainty.

1.3. Outline of work and summary of results. In what follows, we assume a particular form for the relaxation modulus that depends on four parameters and allows for an incremental interpolation between the viscous and viscoelastic regimes. In section 2, we rigorously establish a sequence of essential properties of the GLE. The $\big[M(t) \overset{GLE}{\longleftrightarrow} \widetilde{G}_r(s)\big]$ relationship appears in Theorem 2.4. The form of the relationship that appears in this theorem is identical to the one that appears in Mason and Weitz [27], for example. However, our proof is different than what appears in the microrheology literature and relies on a result that is discussed in Pavliotis [36]. In fact, much of the analysis in the related microrheology literature relies on the assumption that the noise term $F(t)$ in (9) is independent of the velocity process, but in Theorem 2.7 we show that this is not true for stationary solutions of the GLE. This independence assumption dates back at least to Kubo's original paper on the GLE [20] and appears in many seminal works [38, 27, 28, 31, 39, 17] that seek to relate the GLE's memory kernel to its MSD. The difference between the models is a consequence of different specifications for the initial condition of the GLE. We explore this difference in detail in section 2.2. To summarize, we find that the model we work with produces a joint process $\{V(t), F(t)\}_{t\geq 0}$ that is stationary in time, while the prevailing version in the microrheology literature does not. See Theorem 2.7 and Proposition 2.8.

Nevertheless, because Theorem 2.4 holds, the $\big[M(t) \overset{GLE}{\longleftrightarrow} \widetilde{G}_r(s)\big]$ relationship is correct and the standard microrheology protocol used to reconstruct fluid properties from microparticle movement is theoretically sound. We proceed in section 3 to characterize the degree of error that is introduced by each link in the chain (13). We seek to characterize the degree of uncertainty that arises from each step, first assuming perfect knowledge of $\widetilde{G}_r(s)$ and then analyzing the impact of limited observations. The theme that arises throughout the analysis is that, while there is significant error in the estimation of individual parameters, the reconstruction of $G'(\omega)$ and $G''(\omega)$ is remarkably robust in the frequency range that corresponds to the time domain observation window.

2. Generalized Langevin Equation. In this section, we lay out some basic properties of the GLE. For simplicity we assume that $X(t)$ refers to a particle's x-coordinate and so all processes below are one-dimensional:

Generalized Langevin Equation

$$m\mathrm{d}V(t) = \big(-\gamma V(t) - \beta(K^+ * V)(t) + \sqrt{c\beta}F(t)\big)\mathrm{d}t + \sqrt{2c\gamma}\,\mathrm{d}W(t), \tag{14}$$

where $K \in L^1(\mathbb{R})$ is positive definite, $K^+(t) := K(t)1_{t\geq 0}$, $*$ denotes the convolution, and defining $\|K^+\|_1 := \int_{\mathbb{R}} |K^+(t)|dt$,

$$\gamma = 6\pi a\eta_s, \quad \beta = \frac{6\pi a\eta_p}{\|K^+\|_1}, \quad \text{and} \quad c = k_B T. \tag{15}$$

This is the velocity process associated with the shear relaxation modulus

$$G_r(t) = \eta_s \delta(t) + \frac{\eta_p}{\|K^+\|_1} K^+(t). \tag{16}$$

Meanwhile $F(t)$ is a stationary, mean-zero, Gaussian process satisfying

$$\mathbb{E}(F(t)F(s)) = K(t-s). \tag{17}$$

When K can be expressed as a sum of exponential functions, we say it is in the Prony series class:

$$\mathscr{K}_{\text{Prony}} := \left\{ K \,:\, K(t) = \sum_{n=0}^{N-1} G_n e^{-|t|/\tau_n}, \text{ where } G_n, \tau_n > 0 \text{ for all } n \right\}. \tag{18}$$

We will typically work with a subset of the Prony series class called the generalized Rouse kernels.

DEFINITION 2.1. *We say that $K \in \mathscr{K}_{Rouse}$ if for some $N \in \mathbb{N}$, $\nu \geq 1$, and $\tau_0 > 0$, we have*

$$K(t) = \frac{1}{N} \sum_{n=0}^{N-1} e^{-|t|/\tau_n}, \text{ where } \tau_n = \tau_0 \Big(\frac{N}{N-n} \Big)^{\nu}. \tag{19}$$

We call $\{\tau_n\}_{n=0}^{N-1}$ the generalized Rouse spectrum *of relaxation times* with shape parameter ν.

Note that when $K \in \mathscr{K}_{\text{Rouse}}$, $\|K^+\|_1 = \langle \tau_n \rangle := \big(\sum_n \tau_n \big)/N$.

THEOREM 2.2. *Suppose that $K \in \mathscr{K}_{Prony}$. Then there exists a Gaussian, mean-zero, stationary process $V(t)$ satisfying the GLE* (14)*, and it has the spectral density*

$$\widehat{\rho}(\omega) = \frac{c\big(2\gamma + \beta \widehat{K}(\omega)\big)}{|mi\omega + \gamma + \beta \widehat{K^+}(\omega)|^2}. \tag{20}$$

Moreover, the sample paths of V are continuous almost surely and $\mathbb{E}\big(V(0)^2\big) = k_B T/m$.

Proof. The construction of the solution and almost sure continuity are established in [33]. If K is a sum of exponentials, then existence and regularity were established in [8] and the proof that equipartition of energy (see (10)) is satisfied is given in [15, 13]. ∎

Using ϖ to denote elements of the probability space $(\Omega, \mathscr{F}, \mathbb{P})$ on which V is defined, let Ω_c be the probability one event such that for all $\varpi \in \Omega_c$, $(V(t;\varpi))_{t\in\mathbb{R}}$ is continuous. For $t \geq 0$, define $X(t)$ by

$$X(t\,;\varpi) := \begin{cases} \int_0^t V(t'\,;\varpi) \mathrm{d}t', & \varpi \in \Omega_c, \\ 0 & \text{otherwise.} \end{cases} \tag{21}$$

The dynamics of a single-mode Maxwell model are described at length by Grimm, Jeney, and Franosch [11]. While there is a nonlinear feature in the MSD of the position process for such a process, it has been established that *many* modes are necessary to produce persistent anomalous subdiffusive behavior [21, 18, 30]. However, if there are finitely many modes, the MSD is always eventually linear, so we call such behavior *transient anomalous diffusion*. This can be rigorously stated as follows. (See [33] for proof.)

THEOREM 2.3 (transient anomalous diffusion). *Let $M(t) := \mathbb{E}\big(X^2(t)\big)$ be the MSD of $(X(t))_{t\geq 0}$. Then for all $K \in \mathscr{K}_{Prony}$, the associated particle process $\big(X(t), V(t)\big)$ has MSD $M(t) := \mathbb{E}\big(X^2(t)\big)$ satisfying*

$$\lim_{t\to\infty} \frac{M(t)}{t} = C \in (0,\infty). \tag{22}$$

However, suppose that the sequence of particle processes $\{X_N(t), V_N(t)\}_{N\in\mathbb{N}}$ have memory kernels $\{K_N\}_{N\in\mathbb{N}} \subset \mathscr{K}_{Rouse}$ with N terms and common parameters $\tau_0 > 0$ and $\nu > 1$, respectively. Then, denoting $M_N(t) = \mathbb{E}\big(X_N^2(t)\big)$, there exists a function $f(t)$ satisfying

$$\lim_{t\to\infty} f(t)\, t^{-\frac{1}{\nu}} = C' \in (0,\infty) \tag{23}$$

such that for all $T > 0$,

$$\lim_{N\to\infty} \sup_{t\in[0,T]} |M_N(t) - f(t)| = 0. \tag{24}$$

With this backdrop, we proceed to the primary mathematical contributions of this manuscript. First, in Theorem 2.4, we validate the fundamental formula in passive microrheology that relates the Laplace transform of a particle's MSD to its shear relaxation modulus. Subsequently, in section 2.1 we study the version of this theorem (GLE definition and associated proof) that appears in the physics literature.

Our analysis uses Markovian representations of the GLE in which one introduces auxiliary variables to capture the impact of memory on the system. Such an approach was pioneered by Mori [32] and Zwanzig [43]. Two forms of the Markovian GLE have appeared in the mathematics literature recently, and we will find use for each. Some $(N+2)$-dimensional versions have been analyzed recently by Kupferman [21], Goychuk [9, 10], and Ottobre and Pavliotis [35]. We will use a result described in the text by Pavliotis [36]. A $(2N+2)$-dimensional version was introduced by Fricks et al. [8] and allows us to study the relationship between the velocity process and the forcing function F.

THEOREM 2.4 (the connection $M(t) \longleftrightarrow \widetilde{G}_r(s)$). *Let $\big((X(t), V(t))\big)_{t\geq 0}$ be a particle process with shear relaxation modulus $G_r(t)$ of the form (16) that has a memory kernel $K \in \mathscr{K}_{Prony}$. Let $\widetilde{M}(s)$ be the Laplace transform of the associated MSD. Then*

$$6\pi a \widetilde{G}_r(s) = \frac{2c}{s^2\widetilde{M}(s)} - ms. \tag{25}$$

Proof. Suppose that K is a sum of N exponentials. For clearer exposition, define $\lambda_n = \tau_n^{-1}$ for each $n \in \{0,\dots,N-1\}$ and consider the system of SDEs

$$\begin{aligned} m\mathrm{d}V(t) &= \left(-\gamma V(t) - \sum_n \sqrt{\beta G_n} Z_n\right)\mathrm{d}t + \sqrt{2c\gamma}\mathrm{d}W(t), \\ \mathrm{d}Z_n(t) &= \Big(-\lambda_n Z_n(t) + \sqrt{\beta G_n} V(t)\Big)\,\mathrm{d}t + \sqrt{2c\lambda_n}\mathrm{d}W_n(t). \end{aligned} \tag{26}$$

By the same argument presented in Pavliotis [36, Chap. 8], the $V(t)$ defined here is equivalent in distribution to the definition (14). Similar to the form presented by Pavliotis, we claim that

$$p(v,\mathbf{z}) := C\exp\Big(-\frac{1}{2c}\big(mv^2 + |\mathbf{z}|^2\big)\Big) \tag{27}$$

is the stationary distribution of the system (26). To prove this, note that the operator $\mathcal{L}$ associated with this system of SDEs acts on a function $f(v, \mathbf{z})$ that is twice continuously differentiable in all its variables as follows:

$$\begin{aligned}\mathcal{L}f(v,\mathbf{z}) = &-\Big(\frac{\gamma}{m}v + \frac{\sqrt{\beta}}{m}\sum_n \sqrt{G_n}z_n\Big)\frac{\partial f}{\partial v} + \frac{c\gamma}{m^2}\frac{\partial^2 f}{\partial v^2}\\ &+\sum_n \big(\lambda_n z_n + \sqrt{\beta G_n}v\big)\frac{\partial f}{\partial z_n} + c\lambda_n\frac{\partial^2 f}{\partial z_n^2}.\end{aligned}$$

Then, one can show that $p(v, \mathbf{v})$ is the stationary distribution by checking that $\mathcal{L}^* p = 0$, where $\mathcal{L}^*$ is the adjoint of $\mathcal{L}$, satisfying

$$\begin{aligned}\mathcal{L}^* p(v,\mathbf{z}) = &\frac{\partial}{\partial v}\Big(\Big(\frac{\gamma}{m}v + \sum_n \frac{\sqrt{\beta G_n}}{m}z_n\Big)p(v,\mathbf{z})\Big) + \frac{c\gamma}{m^2}\frac{\partial^2 p(v,\mathbf{z})}{\partial v^2}\\ &+\sum_n \frac{\partial}{\partial z_n}\Big(\Big(\lambda_n z_n + \sqrt{\beta G_n}v\Big)p(v,\mathbf{z})\Big) + c\lambda_n\frac{\partial^2 p(v,\mathbf{z})}{\partial z_n^2}.\end{aligned} \tag{28}$$

If the initial condition $(V(0), \mathbf{Z}(0))$ is drawn from the stationary distribution, note that the product structure of $p(v, \mathbf{z})$ yields

$$\begin{aligned}\mathbb{E}(V(0)Z_n(0)) &= \int_{\mathbb{R}^{n+1}} v z_n p(v,\mathbf{z})\mathrm{d}v\mathrm{d}\mathbf{z}\\ &= C\int_{\mathbb{R}} v e^{-\frac{mv^2}{2c}}\mathrm{d}v \int_{\mathbb{R}} z_n e^{-\frac{z_n^2}{2c}}\mathrm{d}z_n \prod_{m\neq n}\Big(\int_{\mathbb{R}} e^{-\frac{z_m^2}{2c}}\mathrm{d}z_m\Big) = 0.\end{aligned} \tag{29}$$

Now, recalling the definition $\rho(t) := \mathbb{E}(V(t)V(0))$ and introducing $\rho_n(t) := \mathbb{E}(Z_n(t)V(0))$, we can multiply (26) through by $V(0)$ and take expectations, resulting in the following system of ODEs:

$$m\dot{\rho}(t) = -\gamma\rho(t) - \sum_n \sqrt{\beta G_n}\rho_n(t), \tag{30}$$

$$\dot{\rho}_n(t) = -\lambda_n\rho_n(t) + \sqrt{\beta G_n}\rho(t). \tag{31}$$

Taking the Laplace transform of (31) yields the solution

$$\widetilde{\rho}_n(s) = \frac{\widetilde{\rho}(s) + \rho_n(0)}{s + \lambda_n}.$$

But from (29), we have that $\rho_n(0) = 0$. Moreover, from Theorem 2.2, $\rho(0) = c/m$. Therefore, substituting what remains in (30), we find that

$$\widetilde{\rho}(s) = \frac{m\rho(0)}{ms + \gamma + \sum_n \beta G_n \frac{1}{s+\lambda_n}} = \frac{c}{ms + 6\pi a\widetilde{G}_r(s)}. \tag{32}$$

To complete the proof we note that $\rho(t)$ is related to the MSD by way of the relation

$$M(t) = 2\int_0^t (t - t')\rho(t')\mathrm{d}t'. \tag{33}$$

This equation appears in Reif [38, Chap. 15], for example. It follows that $\widetilde{\rho}(s) = s^2\widetilde{M}(s)/2$. Equation (25) follows immediately. ∎

2.1. A comment on $\mathbb{E}(F(t)V(0))$. In order to derive the relationship between the shear relaxation modulus and the MSD (Theorem 2.4), arguments in the physics literature typically rely on an assumption that turns out not to be true for the form of the GLE we are studying. The issues arise in the specification of the initial condition for the GLE. To be mathematically rigorous, the initial condition of an integro-differential equation should contain information about its entire history. In many of the canonical references on the GLE, Mason and Weitz [27], Mason [28], Morgado et al. [31], Squires and Mason [39], and Kneller [17], the GLE is defined slightly differently than the informal version of the GLE we presented in (9). The lower limit of integration for the convolution term is zero in these references, rather than negative infinity. In the notation we introduced earlier, the Mason and Weitz version of the GLE can be written

$$\text{Mason and Weitz [27]:} \quad m\dot{V}(t) = -\beta\int_0^t K(t-t')V(t')\mathrm{d}t' + \sqrt{c\beta}F(t), \tag{34}$$

where β and $K(t)$ are defined in (15) and (16), $F(t)$ is a mean-zero Gaussian process with autocovariance $\mathbb{E}(F(t+h)F(h)) = K(t)$, and $V(0) \sim N(0, c/m)$ is independent of $F(0)$. We note that for finite sums of exponentials, it has recently been shown that solutions to (34) are differentiable (see [33, Thm. 5.6]), so the time derivative notation is appropriate. Formally, the authors multiply (34) through by $V(0)$ and take expectations. It follows that $\rho(t) := \mathbb{E}(V(t)V(0))$ must satisfy the integro-differential equation

$$m\dot{\rho}(t) = -\beta\int_0^t K(t-t')\rho(t')\mathrm{d}t' + \sqrt{c\beta}\,\mathbb{E}(F(t)V(0))\,. \tag{35}$$

Applying the Laplace transform, the authors solve for $\widetilde{\rho}(s)$,

$$\widetilde{\rho}(s) = \frac{m\rho(0)}{ms + \beta\widetilde{K}(s)} + \frac{\sqrt{c\beta}\mathscr{L}[\mathbb{E}(F(t)V(0))](s)}{ms + \beta\widetilde{K}(s)}.$$

Then, it is generally *assumed* that $\mathbb{E}(F(t)V(0)) = 0$ for all t so that the last term vanishes. In what follows, we will show that $\mathbb{E}(F(t)V(0)) \neq 0$ for stationary solutions to the GLE (Theorem 2.7). On the other hand, in section 2.2 we show that the covariation of F and V are more nuanced for the Mason and Weitz definition.

In order to analyze $\mathbb{E}(F(t)V(0))$ we need to use a different Markovian representation of the GLE than was used in Theorem 2.4. This is because the non-Markovian noise $F(t)$ is not explicitly represented in (26). However, using a mathematically equivalent form of the GLE, similar to what was used by Fricks et al. [8], we can find an explicit formula for $\mathbb{E}(F(t)V(0))$ and show that it is nonzero for stationary solutions to the GLE. We begin by defining what we call the Fricks representation of the GLE; see (36). We find its stationary distribution in Proposition 2.5, and in Proposition 2.6 we show that it is equivalent to the system (26). Then, in Theorem 2.7, we show that $\mathbb{E}(F(t)V(0)) \neq 0$.

Let $\{U(t), Y_n(t), F_n(t)\}_{t\geq 0}$, $n \in \{1, \ldots, N\}$, be the solution to the system of equations

$$\begin{aligned} m\mathrm{d}U(t) &= -\gamma U(t) - \sum_n \sqrt{\beta G_n}Y_n(t) + \sum_n \sqrt{\beta G_n}F_n(t)\mathrm{d}t + \sqrt{2c\gamma}\mathrm{d}W(t), \\ \mathrm{d}Y_n(t) &= -\lambda_n Y_n(t) + \sqrt{\beta G_n}U(t)\mathrm{d}t, \\ \mathrm{d}F_n(t) &= -\lambda_n F_n(t) - \sqrt{2c\lambda_n}\mathrm{d}W_n(t), \end{aligned} \tag{36}$$

where the $\{W_n\}_{t\geq 0}$ are i.i.d. standard Brownian motions. We introduce the following notation to deal with the correlation structure of this system:

$$\begin{aligned} \varphi_{uu}(t) &:= \mathbb{E}\big(U(t)^2\big)\,, \\ \varphi_{uy_n}(t) &:= \mathbb{E}(U(t)Y_n(t))\,, \quad \varphi_{uf_n}(t) := \mathbb{E}(U(t)F_n(t))\,, \\ \varphi_{y_ny_k}(t) &:= \mathbb{E}(Y_n(t)Y_k(t))\,, \quad \varphi_{y_nf_k}(t) := \mathbb{E}(Y_n(t)F_k(t))\,, \\ \varphi_{f_nf_k}(t) &:= \mathbb{E}(F_n(t)F_k(t))\,. \end{aligned} \tag{37}$$

We will use the notation $\bar{\varphi}_{[\cdots]}$ for the steady-state values corresponding to each of these quantities.

PROPOSITION 2.5. *Suppose that $\{U(t), Y_n(t), F_n(t)\}_{t\geq 0}$ satisfies* (36)*. Then there exists a unique stationary distribution, which is Gaussian with mean zero and covariances given by*

$$\begin{aligned} \bar{\varphi}_{uu} &= c/m; \quad \bar{\varphi}_{f_nf_k} = c\delta_{nk}, \\ \bar{\varphi}_{uy_n} &= c\sqrt{\beta G_n}/\big(m\lambda_n + \gamma + \beta\widetilde{K}^+(\lambda_n)\big), \\ \bar{\varphi}_{uf_n} &= c\sqrt{\beta G_n}/\big(m\lambda_n + \gamma + \beta\widetilde{K}^+(\lambda_n)\big), \\ \bar{\varphi}_{y_ny_k} &= \big(\sqrt{\beta G_k}\,\bar{\varphi}_{uy_n} + \sqrt{\beta G_n}\,\bar{\varphi}_{uy_k}\big)/(\lambda_n + \lambda_k), \\ \bar{\varphi}_{y_nf_k} &= \sqrt{\beta G_n}\bar{\varphi}_{uf_k}/(\lambda_n + \lambda_k). \end{aligned} \tag{38}$$

Proof. Because (2.5) is a linear system of SDEs, if the initial condition is jointly Gaussian, the law will be jointly Gaussian as well. That the stationary distribution has mean zero follows from taking expectations throughout (36), setting the time derivative to zero, and solving.

We take a similar approach when assessing the second moments. Applying Itô's formula to each product in the system of equations (36) and taking expectations yields the following system of ODEs:

$$\frac{m}{2}\dot{\varphi}_{uu} = -\gamma\varphi_{uu} + \frac{c\gamma}{m} - \sum_k \sqrt{\beta G_k}\big(\varphi_{uy_k} - \varphi_{uf_k}\big), \tag{39}$$

$$m\dot{\varphi}_{uy_n} = -\big(m\lambda_n + \gamma\big)\varphi_{uy_n} + m\sqrt{\beta G_n}\varphi_{uu} - \sum_k \sqrt{\beta G_k}\big(\varphi_{y_ny_k} - \varphi_{y_nf_k}\Big), \tag{40}$$

$$m\dot{\varphi}_{uf_n} = -\Big(m\lambda_n + \gamma\Big)\varphi_{uf_n} - \sum_k \sqrt{\beta G_k}\big(\varphi_{y_kf_n} - \varphi_{f_nf_k}\big), \tag{41}$$

$$\dot{\varphi}_{y_ny_k} = -\big(\lambda_n + \lambda_k\big)\varphi_{y_ny_k} + \big(\sqrt{\beta G_k}\varphi_{uy_n} + \sqrt{\beta G_n}\varphi_{uy_k}\big), \tag{42}$$

$$\dot{\varphi}_{y_nf_k} = -\big(\lambda_n + \lambda_k\big)\varphi_{y_nf_k} + \sqrt{\beta G_n}\varphi_{uf_k}, \tag{43}$$

$$\dot{\varphi}_{f_nf_k} = -\big(\lambda_n + \lambda_k\big)\varphi_{f_nf_k} + 2c\lambda_n\delta_{nk}, \tag{44}$$

where in (44), δ_{nk} is the Kronecker δ-function. For each pair, the stationary covariance can be obtained by taking $\bar{\varphi}_{[\cdots]} = \lim_{t\to\infty}\varphi_{[\cdots]}(t)$, or by setting all derivatives on the left-hand side to zero and solving the resulting set of linear equations. We take the latter approach.

First, we note that (44) is autonomous so

$$\bar{\varphi}_{f_nf_k} = c\delta_{nk}. \tag{45}$$

Next we observe that, by Theorem 2.2, $m\bar{\varphi}_{uu} = c$. This cancels the first two terms of the steady-state version of (39). The remainder of our analysis rests on establishing

the following Ansatz, which would serve to eliminate the final term of (39):

$$\text{Auxiliary Balance Condition:} \quad \bar{\varphi}_{uy_n} = \bar{\varphi}_{uf_n} \text{ for all } n. \tag{46}$$

From (43) and (42) we see that

$$\bar{\varphi}_{y_n f_k} = \frac{\sqrt{\beta G_n}}{\lambda_n + \lambda_k}\bar{\varphi}_{uf_k} \quad \text{and} \quad \bar{\varphi}_{y_n y_k} = \frac{\sqrt{\beta G_k}\bar{\varphi}_{uy_n} + \sqrt{\beta G_n}\bar{\varphi}_{uy_k}}{\lambda_n + \lambda_k}. \tag{47}$$

Substituting the first relation from (47) and (45) into (41) we have

$$(m\lambda_n + \gamma)\bar{\varphi}_{uf_n} = \sum_k \left(-\frac{\beta G_k}{\lambda_n + \lambda_k}\bar{\varphi}_{uf_n} + c\sqrt{\beta G_k}\delta_{nk} \right),$$

which simplifies to

$$\big(m\lambda_n + \gamma + \beta\widetilde{K}^+(\lambda_n)\big)\bar{\varphi}_{uf_n} = c\sqrt{\beta G_n}. \tag{48}$$

We solve for φ_{uy_n} by substituting the second relation from (47) into (40). Again using $m\bar{\varphi}_{uu} = c$, we have

$$\big(m\lambda_n + \gamma\big)\bar{\varphi}_{uy_n} = c\sqrt{\beta G_n} - \sum_k \sqrt{\beta G_k}\left(\frac{\sqrt{\beta G_k}\bar{\varphi}_{uy_n} + \sqrt{\beta G_n}\bar{\varphi}_{uy_k}}{\lambda_n + \lambda_k} - \frac{\sqrt{\beta G_n}\bar{\varphi}_{uf_k}}{\lambda_n + \lambda_k} \right).$$

If we assume the Auxiliary Balance Condition (46) holds, then for each k, $\bar{\varphi}_{uy_k} = \bar{\varphi}_{uf_k}$ and this simplifies to

$$\big(m\lambda_n + \gamma + \beta\widetilde{K}^+(\lambda_n)\big)\bar{\varphi}_{uy_n} = c\sqrt{\beta G_n}. \tag{49}$$

Finally, we need to check that the resulting values for $\bar{\varphi}_{uy_k}$ and $\bar{\varphi}_{uf_k}$ actually satisfy the Auxiliary Balance Condition. Consulting (49) and (48), we see that they do. Since we have solved a linear system of equations with full rank, the solution is unique, and the proof is complete. ∎

In Figure 2 we display a time evolution of a subset of the cross-variation processes. The solid lines with `x`'s in both panels correspond to solutions to the system (39)–(45) with initial conditions set to be the steady state. The steady state of (39) is displayed in black, and that of the sum over the system of equations (41) in gray. The solid curves without `x`'s correspond to solutions to these equations with the initial condition chosen to comply with the Mason and Weitz version of the GLE (34) in Figure 2a and a slight perturbation of those initial conditions in Figure 2b. These plots demonstrate a fact we will prove in section 2.2, that the Mason and Weitz definition of the joint process $\{V(t), F(t)\}_{t\geq 0}$ is not stationary. The perturbation made to the initial conditions in Figure 2b were chosen to violate the Auxiliary Balance Condition. Although it is not depicted, Auxiliary Balance is restored as time increases. Meanwhile, this type of perturbation results in $\mathbb{E}\big(V(t)^2\big)$ departing from its stationary state before returning at a later time.

The two Markovian systems (26) and (36) can be seen to be equivalent by noting that $Z_n = Y_n - F_n$ yields the same system. For example, using the structure of the stationary distribution laid out in Proposition 2.5, we can show that for all $1 \leq n, k \leq N$ we have that for stationary solutions of (36),

$$\mathbb{E}(Y_n - F_n) = 0 \quad \text{and} \quad \mathbb{E}((Y_n - F_n)(Y_k - F_k)) = c\delta_{nk}.$$

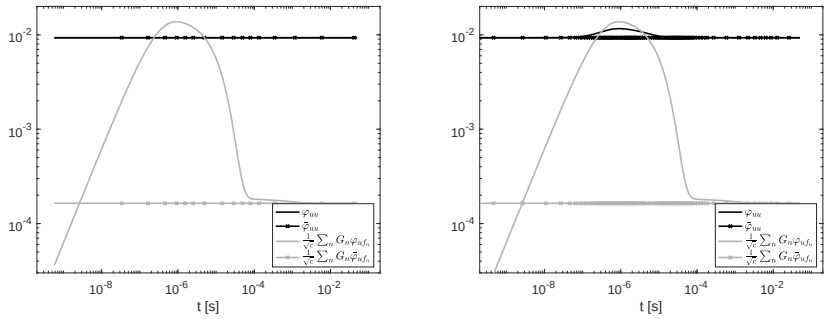

(a) Mason & Weitz GLE (b) Perturbed Mason & Weitz GLE

FIG. 2. Cross-variation of auxiliary modes. *Solutions and steady-states for the system of ODEs capturing the cross-variation of variables in the Fricks representation* (36) *of the Mason and Weitz version of the GLE* (9). *($N = 2$, $\tau_0 = 10^{-3}s$, $\eta_s = 10^{-2}g/(cm\ s)$, $\eta_p/\tau_{avg} = 10^3 g/(cm\ s^2)$.) In both cases, the initial velocity is Gaussian with mean zero and variance c/m. In the* left panel, *all auxiliary variables are set to zero at time zero as in section* 2.1. *In the* right panel, *we set $Y_1(0)$ to be a Gaussian random variable with variance 10^{-12}. In both cases the gray curve, $E(V(t)F(t))$, analyzed in terms of Propositions* 2.5 *and* 2.6, *departs from its initial zero value and converges to its steady state (gray with $\mathbf{x}$'s). In the* left panel $\mathbb{E}(V(t)^2)$ *(solid black) is seen to be constant, while in the* right panel *the perturbation in the initial condition causes a perturbation in the time series for $\mathbb{E}(V(t)^2)$.*

The relationship is actually stronger than this distributional equivalence. In the following proposition we show that if the two Markovian systems are driven by the same noise processes, then the resulting velocity processes are equal to each other pathwise almost surely.

PROPOSITION 2.6. *Let $u, \{y_n\}$, and $\{f_n\}$ be drawn from the stationary distribution of* (36). *Let $v = u$ and $z_n = y_n - f_n$ and suppose that $\{V(t), Z_n(t)\}_{t\geq 0}$ satisfies* (26) *with initial conditions $\{V(0) = v, Z_n(0) = z_n\}$ while $\{U(t), Y_n(t), F_n(t)\}_{t\geq 0}$ satisfies* (36) *with initial conditions $\{U(0) = u, Y_n(0) = y_n, F_n(0) = f_n\}$. Then, for any $T > 0$,*

$$\sup_{t\in[0,T]} |V(t;\varpi) - U(t;\varpi)| = 0 \text{ for almost all } \varpi \in \Omega.$$

Proof. We can rewrite the velocity portions of (26) and (36) as integral equations and use Duhamel's formula for the auxiliary variables as follows:

$$\begin{aligned} V(t) &= v - \sum_n \sqrt{\beta G_n} \int_0^t Z_n(s)\mathrm{d}s + \sqrt{2c\gamma}W(t), \\ Z_n(t) &= e^{-\lambda_n t} z_n + \sqrt{\beta G_n} \int_0^t e^{-\lambda_n (t-s)} V(s)\mathrm{d}s + \sqrt{2c\lambda_n} \int_0^t e^{-\lambda_n (t-s)} \mathrm{d}W_n(s), \end{aligned} \tag{50}$$

and

$$\begin{aligned} U(t) &= u - \sum_n \sqrt{\beta G_n} \int_0^t Y_n(s)\mathrm{d}s + \sum_n \sqrt{\beta G_n} \int_0^t F_n(s)\mathrm{d}s + \sqrt{2c\gamma}W(t), \\ Y_n(t) &= e^{-\lambda_n t} y_n + \sqrt{\beta G_n} \int_0^t e^{-\lambda_n (t-s)} U(s)\mathrm{d}s, \\ F_n(t) &= e^{-\lambda_n t} f_n - \sqrt{2c\lambda_n} \int_0^t e^{-\lambda_n (t-s)} \mathrm{d}W_n(s). \end{aligned} \tag{51}$$

Because the integrands are deterministic and differentiable in the stochastic integrals above, they can be interpreted pathwise (ϖ-by-ϖ) using Young integrals [1] for all $\varpi \in \Omega_0 \subset \Omega$ where $\mathbb{P}\{\Omega_0\} = 1$.

Now, for all $\varpi \in \Omega_0$, define

$$\hat{V}(t;\varpi) = V(t;\varpi) - U(t;\varpi) \quad \text{and} \quad \hat{Z}_n(t;\varpi) = Z_n(t;\varpi) - (Y_n(t;\varpi) - F_n(t;\varpi)). \tag{52}$$

Then

$$\hat{V}(t;\varpi) = -\sum_n \sqrt{\beta G_n} \int_0^t \hat{Z}_n(s;\varpi)\mathrm{d}s \text{ and } \hat{Z}_n(t;\varpi) = \sqrt{\beta G_n} \int_0^t e^{-\lambda_n(t-s)} \hat{V}(s;\varpi)\mathrm{d}s.$$

Substituting the $\hat{Z}_n$'s into the equation for $\hat{V}$, recognizing K, and differentiating both sides yields the integro-differential equation

$$\frac{d}{dt}\hat{V}(t;\varpi) = -\beta \int_0^t K(t-s)\hat{V}(s;\varpi)\mathrm{d}s$$

with initial condition $\hat{V}(0;\varpi) = 0$, which implies $\hat{V}(t) \equiv 0$ almost surely. ∎

THEOREM 2.7. *Let $\{V(t)\}_{t\geq 0}$ be a particle velocity process with shear relaxation modulus $G_r(t)$ of the form* (16) *that has a memory kernel $K \in \mathscr{K}_{Prony}$. If $V(t)$ is a stationary solution to* (14)*, then for all $t, h \geq 0$,*

$$\mathbb{E}(F(t+h)V(h)) = \sum_n \frac{G_n\sqrt{\beta c}}{m\tau_n^{-1} + 6\pi a \widetilde{G}_r(\tau_n^{-1})} e^{-t/\tau_n}. \tag{53}$$

Proof. Using the preceding results, it suffices to study the GLE represented by the system (36), noting that

$$\mathbb{E}(F(t+h)V(h)) = \mathbb{E}(F(t+h)U(h)) = \frac{1}{\sqrt{c}} \sum_n \sqrt{G_n}\mathbb{E}(F_n(t+h)U(h)) \tag{54}$$

for $t \geq 0$.

Let $h \geq 0$ be given. We define the following time-dependent quantities:

$$\begin{aligned} \rho(t;h) := \mathbb{E}(U(t+h)U(h))\,,\ \rho_{y_n}(t;h) := \mathbb{E}(Y_n(t+h)U(h))\,, \\ \text{and } \rho_{f_n}(t;h) := \mathbb{E}(F_n(t+h)U(h))\,. \end{aligned} \tag{55}$$

When $h = 0$, we will generally suppress its appearance in the notation ($\rho(t) := \rho(t;0)$).

If we multiply (36) through by $U(h)$ and take expectations, we have the system of ODEs

$$\begin{aligned} m\dot{\rho}(t;h) &= -\gamma\rho(t;h) - \sum_n \sqrt{\beta G_n}\big(\rho_{y_n}(t;h) - \rho_{f_n}(t;h)\big), \\ \dot{\rho}_{y_n}(t;h) &= -\lambda_n\rho_{y_n}(t;h) + \sqrt{\beta G_n}\rho(t;h), \\ \dot{\rho}_{f_n}(t;h) &= -\lambda_n\rho_{f_n}(t;h). \end{aligned}$$

Note that the Laplace transforms of the latter two equations can be written in the form

$$\widetilde{\rho}_{y_n}(s;h) = \frac{\sqrt{\beta G_n}\,\widetilde{\rho}(s;h) + \varphi_{uy_n}(h)}{s+\lambda_n} \quad \text{and} \quad \widetilde{\rho}_{f_n}(s;h) = \frac{\varphi_{uf_n}(h)}{s+\lambda_n}. \tag{56}$$

Recalling that $\widetilde{K^+}(s) = \sum_n G_n/(s+\lambda_n)$, we find that

$$\widetilde{\rho}(s;h) = \frac{m\rho(0;h)}{ms+\gamma+\beta\widetilde{K^+}(s)} - \sum_n \frac{\sqrt{\beta G_n}\big(\varphi_{uy_n}(h) - \varphi_{uf_n}(h)\big)}{\big(ms+\gamma+\beta\widetilde{K^+}(s)\big)(s+\lambda_n)}. \tag{57}$$

The Auxiliary Balance Condition (46) implies that the sum is zero when considering stationary solutions of (36). (We note that this is a second proof of Theorem 2.4, having re-established the form of $\widetilde{\rho}(s)$ written in (32) with $\rho(0) = c/m$.)

Using (48), we have that

$$\widetilde{\rho}_{f_n}(s;h) = \frac{1}{s+\lambda_n}\frac{c\sqrt{\beta G_n}}{m\lambda_n+\gamma+\beta\widetilde{K^+}(\lambda_n)}.$$

Substituting this into (54) and inverting the Laplace transform yields the desired result. ∎

2.2. Understanding the Mason and Weitz version of the GLE. To complete our discussion, we revisit the form of the GLE usually presented in the physics literature (35) where the convolution is taken from time 0 to ∞ rather than from $-\infty$ to ∞. We will show that this version of the GLE can be expressed in terms of the system (36); that the associated velocity process satisfies $\mathbb{E}(V(t)V(0)) = \rho(t)$ for all $t > 0$; and that the noise-velocity pair satisfies $\mathbb{E}(F(t)V(0)) = 0$ for all t. Moreover, there is substantial numerical evidence that $\mathbb{E}(V(t+h)V(h)) = \rho(t)$, which would state that this $V(t)$ is a stationary Gaussian process equal in law to the stationary solutions studied in the previous section. This is an example of two processes being equivalent in law, but not being pathwise equivalent.

However, while the velocity processes have the same law we will show that there is an important sense in which solutions to (35) are not stationary. Namely, the velocity-noise pair $\{V(t), F(t)\}_{t\geq 0}$ is not jointly stationary because we can prove that for $h > 0$ sufficiently large, $\mathbb{E}(F(t+h)V(h)) > 0 \neq \mathbb{E}(F(t)V(0))$.

Let $m, \beta, c > 0$ and let $\{F(t)\}_{t\in\mathbb{R}}$ be a stationary, mean-zero Gaussian process with $\mathbb{E}(F(t+s)F(s)) = K(t)$ for all t, s. For $h \geq 0$, define the process $\{V_h(t)\}_{t\geq -h}$ as follows:

$$m\dot{V}_h(t) = -\beta\int_{-h}^{t} K(t-s)V_h(s)\mathrm{d}s + F(t), \tag{58}$$

where $V_h(-h) = v \sim N(0, c/m)$. This equation provides an interpolation between the Mason and Weitz version of the GLE (34) ($h = 0$) and our definition of stationary solutions to (14) ($h = -\infty$).

We have the following proposition.

PROPOSITION 2.8. *Let $\{F(t)\}_{t\in\mathbb{R}}$ and $\{V_h(t)\}_{t\geq -h}$ be defined as in* (58) *with a memory kernel $K \in \mathscr{K}_{Prony}$. Then there exists an $h > 0$ sufficiently large such that*

$$\mathbb{E}(F(t)V_h(0)) > 0. \tag{59}$$

Proof. In order to use the structure utilized in Theorem 2.7, define $\{V_h^*(t)\}_{t\geq 0}$ and let $\{V_h^*(t)\}_{t\in\mathbb{R}}$ be time-shifted versions of the velocity and the forcing: $V_h^*(t) := V_h(t-h)$ and $F_h^*(t) = F(t-h)$. Then for all $t \geq 0$

$$m\dot{V}_h^*(t) = -\beta\int_{-h}^{t} K(t-s)V_h^*(s)\mathrm{d}s + F_h^*(t).$$

Noting that F_h^* is equivalent in law to F, it follows that

$$\mathbb{E}(F(t)V_h(0)) = \mathbb{E}(F_h^*(t+h)V_h^*(h)) = \frac{1}{\sqrt{c}}\sum_n \sqrt{G_n}\rho_{f_n}(t;h),$$

where $\rho_{f_n}(t;h)$ is as defined in (55). This implies that

$$\mathbb{E}(F(t)V_h(0)) = \frac{1}{c}\sum_n \sqrt{G_n}\varphi_{uf_n}(h)e^{-\lambda_n t}.$$

When $h = 0$, then this quantity is zero, implying that $\mathbb{E}(F(t)V_0(0)) = 0$ for all $t > 0$. However, there exists a unique stationary solution for the system (39)–(44), solutions are continuous (since it is a linear system), and $\lim_{t\to\infty}\varphi_{uf_n}(t) > 0$. Therefore (59) follows. ∎

3. Parameter estimation and a Monte Carlo visualization of uncertainty for rheological properties.

3.1. Parametric inference imposes small- and large-ω asymptotics. For the work we present in this section, we work within the $\mathscr{K}_{\text{Prony}}$ framework for modeling viscoelastic diffusion. It is important to note that this imposes a structure on the storage and loss moduli G' and G''.

PROPOSITION 3.1. *Let $K \in \mathscr{K}_{Prony}$. Then the storage and loss moduli have the following asymptotic properties:*

$$\lim_{\omega\to 0}\frac{G'(\omega)}{\omega^2} = \frac{\eta_p\langle\tau_n^2\rangle}{\langle\tau_n\rangle}, \qquad \lim_{\omega\to\infty} G'(\omega) = \frac{\eta_p}{\langle\tau_n\rangle}, \tag{60}$$

$$\lim_{\omega\to 0}\frac{G''(\omega)}{\omega} = \eta_s + \frac{\eta_p}{\langle\tau_n\rangle}, \qquad \lim_{\omega\to\infty}\frac{G''(\omega)}{\omega} = \eta_s, \tag{61}$$

where we adopt the notation

$$\langle\tau_n^p\rangle := \sum_{n=0}^{N-1} G_n\tau_n^p, \tag{62}$$

where $p > 0$.

Proof. If $K \in \mathscr{K}_{\text{Prony}}$, then

$$\widehat{K^+}(\omega) = \sum_n \frac{G_n\tau_n}{1+i\omega\tau_n}. \tag{63}$$

From the definitions of the storage and loss moduli (4), and the definition of G_r (16), we have

$$G'(\omega) = \frac{\eta_p}{\langle\tau_n\rangle}\sum_n \frac{G_n\tau_n^2\omega^2}{1+\tau_n^2\omega^2} \quad \text{and} \quad G''(\omega) = \eta_s\omega + \frac{\eta_p}{\langle\tau_n\rangle}\sum_n \frac{G_n\tau_n\omega}{1+\tau_n^2\omega^2}. \tag{64}$$

The asymptotic expressions follow immediately. ∎

Once we impose the Generalized Rouse Spectrum for the memory kernel, we can describe a feature in G' and G'' that arises from the particle's transient anomalous diffusion.

PROPOSITION 3.2. *Let $\nu > 1$, $\tau_0 > 0$, and $\eta_s > 0$ be given. For each $N \in \mathbb{N}$, let $K_N(t) \in \mathscr{K}_{Rouse}$ be the associated generalized Rouse memory kernel with N exponential terms. For every $t > 0$, define $K(t) := \lim_{N\to\infty} K_N(t)$ and let G' and G'' be the storage and loss moduli associated with the memory kernel $K(t)$. Moreover, suppose that $\eta_p = \eta_p(N)$ in such a way that $\lim_{N\to\infty} \eta_p(n)/\langle\tau_n(N)\rangle = G_0 \in (0,\infty)$. Then*

$$\lim_{\omega\to 0} \frac{G'(\omega)}{\omega^{\frac{1}{\nu}}} = \frac{1}{\nu} G_0 \tau_0^{\frac{1}{\nu}} C_0(\nu), \qquad \lim_{\omega\to\infty} G'(\omega) = G_0, \tag{65}$$

$$\lim_{\omega\to 0} \frac{G''(\omega)}{\omega^{\frac{1}{\nu}}} = \frac{1}{\nu} G_0 \tau_0^{\frac{1}{\nu}} C_1(\nu), \qquad \lim_{\omega\to\infty} \frac{G''(\omega)}{\omega} = \eta_s. \tag{66}$$

where $C_r := \int_0^\infty \frac{u^r}{u^{1-\frac{1}{\nu}}} \frac{1}{1+u^2} \mathrm{d}u$.

Proof. For $G'(\omega)$ we can rewrite (64) with the generalized Rouse kernel as a Riemann approximation to an integral and take $N \to \infty$:

$$\begin{aligned} G'(\omega) &= \lim_{N\to\infty} \frac{\eta_p}{\langle\tau_n\rangle} \frac{1}{N} \sum_n \frac{\tau_n^2\omega^2}{1+\tau_n^2\omega^2} = G_0 \lim_{N\to\infty} \sum_n \frac{\tau_0^2\omega^2}{\tau_0^2\omega^2 + (n/N)^{2\nu}} \frac{1}{N} \\ &= G_0 \int_0^1 \frac{\tau_0^2\omega^2}{\tau_0^2\omega^2 + x^{2\nu}} \mathrm{d}x. \end{aligned} \tag{67}$$

After the substitution $u = x^\nu/\tau_0\omega$, we have

$$G'(\omega) = \frac{G_0(\tau_0\omega)^{\frac{1}{\nu}}}{\nu} \int_0^{\frac{1}{\tau_0\omega}} \frac{1}{u^{1-\frac{1}{\nu}}} \frac{1}{1+u^2} \mathrm{d}u. \tag{68}$$

The same procedure yields

$$\begin{aligned} G''(\omega) &= \eta_s\omega + \lim_{N\to\infty} \frac{\eta_p}{\langle\tau_n\rangle} \frac{1}{N} \sum_n \frac{\tau_n\omega}{1+\tau_n^2\omega^2} = \eta_s\omega + G_0 \int_0^1 \frac{\tau_0\omega x^\nu}{\tau_0^2\omega^2 + x^{2\nu}} \mathrm{d}x \\ &= \eta_s\omega + \frac{G_0(\tau_0\omega)^{\frac{1}{\nu}}}{\nu} \int_0^{\frac{1}{\tau_0\omega}} \frac{u}{u^{1-\frac{1}{\nu}}} \frac{1}{1+u^2} \mathrm{d}u. \end{aligned} \tag{69}$$

Since both integrands are integrable over $u \in (0,\infty)$ the $\omega \to 0$ limit follows immediately.

To assess the large-ω limit, we return to (67). As ω tends to infinity, the integrand uniformly approaches the constant function one. Therefore $G'(\omega) \to G_0$ as $\omega \to \infty$. Similarly, we see that as $\omega \to \infty$, the integrand in (69) goes to zero uniformly over $x \in [0,1]$, leaving only the term $\eta_s\omega$. ∎

3.2. Current methods; reliance on power law fits. Because power laws are so apparent in pathwise MSDs computed from live data, it is perhaps natural to simply plot the averaged pathwise MSDs on a log-log scale and use linear regression to find the power law with the best fit. Then, assuming the mass is negligible, one would estimate $\widetilde{G}_r(s)$ through (25), setting $m = 0$. First, note that for $\alpha \in (0,1)$, we have $\mathscr{L}\{t^\alpha\}(s) = \Gamma(1+\alpha)s^{-(1+\alpha)}$. Then one would estimate that

$$M(t) = Ct^\alpha \;\text{ implies }\; \widetilde{G}_r(s) \approx \frac{2k_BT}{6\pi aC\Gamma(1+\alpha)s^{1-\alpha}}. \tag{70}$$

Using the relations

$$G'(\omega) = -\omega \operatorname{Im}\big[\widetilde{G}_r(i\omega)\big] \quad \text{and} \quad G''(\omega) = \omega \operatorname{Re}\big[\widetilde{G}_r(i\omega)\big], \tag{71}$$

we have that

$$M(t) = Ct^{\alpha} \ \text{ implies } \begin{cases} G'(\omega) = C' \cos\big(\alpha\pi/2\big)\, \omega^{\alpha}, \\ G''(\omega) = C' \sin\big(\alpha\pi/2\big)\, \omega^{\alpha}, \end{cases} \tag{72}$$

where $C' = k_B T/(3\pi a C \Gamma(1+\alpha))$.

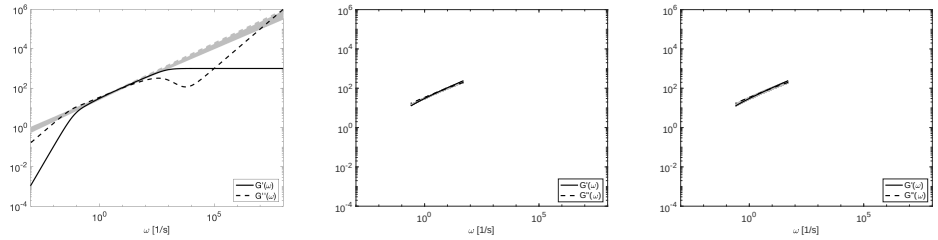

(a) Power Law MSD Fit [12] (b) Mason [28] (c) Dasgupta et al [4]

FIG. 3. Estimated Storage and Loss Moduli using existing methods. *For a fixed parameter set, we simulated* 100 *sets of* 100 *particle paths. For each set of paths, we calculated an ensemble Pathwise MSD and then applied three existing methods for inferring* G' *and* G''*, seen as gray solid and dashed curves. The methodology for these plots is described in sections* 3.4–3.5*. In each case, we see that little information is gained outside a one log-decade range of frequencies.* $N = 100$*,* $\tau_0 = 10^{-3} s$*,* $\eta_s = 10^{-2} g/(cm\ s)$*,* $\eta_p/\tau_{avg} = 10^3 g/(cm\ s^2)$*.*

As noted in Theorem 2.3, for $K \in \mathscr{K}_{\text{Rouse}}$, $\alpha = 1/\nu$. Therefore, the small-ω regime seen in (72) is the same as identified in the $N \to \infty$ limit for a generalized Rouse kernel. In the large-ω limit, however, the $N \to \infty$ limit does not match the pure power law forms for $G'(\omega)$ and $G''(\omega)$. This is because the τ_0 is unchanged in the limit, and for all times smaller than this smallest relaxation time, the fluid is essentially viscous.

In Figure 3a, we display the results of using a pure power law fit of the MSD to infer the storage and loss moduli when the true $G_r(t)$ has a memory kernel in $\mathscr{K}_{\text{Rouse}}$ with 100 terms and $\nu = 2$. We see that the Power Law MSD fit matches the subdiffusive feature of $G'(\omega)$ and $G''(\omega)$ that appears in the range $\omega \in (10^0, 10^2)$ s^{-1}. If N were taken to be larger, the subdiffusive feature would extend in the small-ω range and presumably match the Power Law MSD fit.

In principle, a fully observed MSD will feature multiple power law regimes. For times much smaller than τ_0 the log-log slope should be one. Also, for times much larger than the largest time scale ($\sim \tau_N^{\nu}$) the log-log slope will be one again. The intermediate regime of the logscale MSD will be sublinear. In their original paper on passive microrheology, Mason and Weitz computed a numerical Laplace transform of an ensemble average of Pathwise MSD curves, then used (25) to translate this to $\widetilde{G}_r(s)$. They then fit to a function of the form $\widetilde{G}_r(s) = a_0 + a_1 s + \sum_{j=2}^{J} a_j s^{\nu_j}$ with $(\nu_3, \nu_4, \nu_5) = (-0.55, 0.3, 0.5)$. Invoking analytic continuation, they defined $\widehat{G}_r(\omega) := \widetilde{G}_r(i\omega)$ and then applied the relations (71) to compute G' and G''. From what we have seen in (72), this imposes a small-ω form that has leading order $\omega^{-0.55}$ and a large-ω leading order ω^1.

Concerned about the structure imposed by a parametric model for $\widetilde{G}_r(s)$, Mason introduced a less restrictive method five years later [28]. Essentially, the method is as follows. For each t, one computes a "local" power law fit which we denote $\alpha(t)$. Then, this is translated to an estimate for $\widetilde{G}_r(s)$ using a localized version of (70):

$$\text{Mason [28]:} \quad \widetilde{G}_r(s) \approx \frac{2k_BT}{6\pi asM(1/s)\Gamma(1+\alpha(1/s))}. \tag{73}$$

(Note that the quantity that Mason computes ($\widetilde{G}(s)$) is related to $\widetilde{G}_r(s)$ by $\widetilde{G}(s) = \widetilde{G}_r(s)$.) The form of the approximation follows from the observation that if $M(t) = Ct^\alpha$, then the quantity $Cs^{1-\alpha}$ in the denominator of the right-hand side of (70) can be rewritten as $sM(1/s)$.

Much like the previous methods, Mason's approximation imposes an assumption on the small- and large-ω regimes. In this case, they are set by the local power law fit and the two extremes of the observed MSD. But there is a more subtle assumption that could affect inference. While Mason's method should be sensitive to power law transitions in the MSD form, it relies on the assumption that $\widetilde{M}(s)$ can be approximated by behavior of the MSD in the neighborhood of $t = 1/s$. However, note that since $\widetilde{M}(s) = \int_0^\infty M(t)e^{-st}$, its value is informed by the values of $M(t)$ in a neighborhood of the maximum value of the integrand, $t_*(s) = \arg\max_{t>0}\{M(t)e^{-st}\}$. In particular, if $M(t) = Ct^\alpha$, then $t_*(s) = \alpha/s$. In questions of interest, α is much smaller than one, meaning that Mason's approximation samples a region of M far from the peak of the integrand's contribution. For the same 100 sets of 100 paths, we applied Mason's method to estimate G' and G''. The results are displayed in Figure 3b. We only include values $\{\omega_k\}_{k=1}^{T_N}$ that are of the form $\omega_k = 1/t_k$ where t_k is a time point for which path observations were made.

For observed MSD that is highly curved, Dasgupta et al. proposed a generalization to the local power law fit to account for changes in the curvature [4]. Using a polynomial of degree two to fit the logarithm of the MSD, the authors propose an empirical localized version of (70) to be

$$\text{Dasgupta [4]:} \quad \widetilde{G}_r(s) \approx \frac{2k_BT}{6\pi asM(1/s)\Gamma(1+\alpha(1/s))(1+\beta(1/s)/2)}. \tag{74}$$

Further modified versions of the loss and storage forms (72) are proposed based on a degree two logarithmic fit of $\widetilde{G}_r(s)$. However, for MSD that exhibits multiple time scales but transitions smoothly between the different regimes, this method has the same shortcoming as the local power law fit and does not provide any new information. For illustrative purposes, the reconstruction is given in Figure 3c.

3.3. [$\widetilde{G}_r(s) \longleftrightarrow G^*(\omega)$] Generalized Rouse Spectrum identifiability issues. Uncertainty arises from multiple sources in standard practice for passive microrheology. Some are experimental, like limitations on the camera frame rate ($1/\delta$) and the length of the particle paths (N_T). The conversion from the time domain to frequency space also introduces potential for error that we explore in the next section. In this section, we investigate parameter uncertainty that arises from the Rouse spectrum model itself: namely, while there are no pairs of unidentifiable parameters, there is a strong relationship between the parameters when an error is made. However, the effect on the inferred storage and loss moduli is relatively limited.

To assess the impact of what is sometimes called *practical unidentifiability* [37] among the parameters of the Generalized Rouse Spectrum, we conducted a numerical

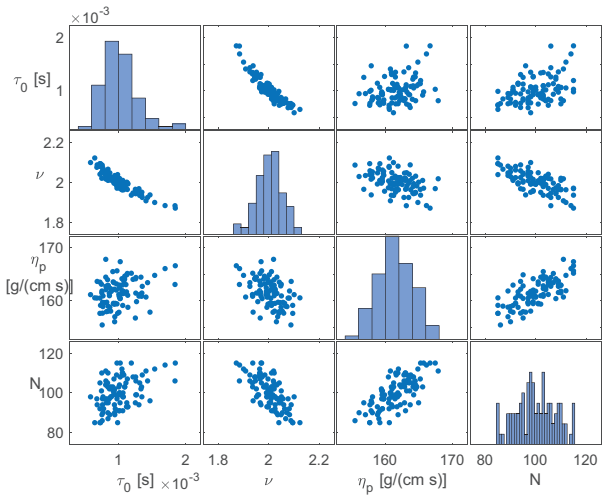

FIG. 4. Parameter relationships for generalized Rouse spectrum model. *For a fixed parameter set, the corresponding function* $\widetilde{G}_r(s)$ *was perturbed* 100 *times and estimated values for* N, τ_0, η_p, ν *were computed according to the procedure described in* (76)*. Histograms of the values are plotted on the diagonal subplots, while scatter plots of each two-parameter combination are on the off-diagonal. The scatter plots show that* (τ_0, ν) *are highly correlated, while none of the other parameters are.* ($N = 100$, $\tau_0 = 10^{-3} s$, $\eta_s = 10^{-2} g/(cm\ s)$, $\eta_p/\tau_{avg} = 10^3 g/(cm\ s^2)$.)

experiment in the spirit of the analysis carried out for cholera transmission pathways by Eisenberg, Robertson, and Tien [5]. In section 3.3.1, we describe a procedure whereby we generated 100 sets of randomly perturbed relaxation moduli and conducted parameter estimation in each case for N, η_p, τ_0, and ν. In Figure 4, we plotted the histograms of the estimated parameters on the diagonal as well as the scatter plots of two sets of estimated parameters on the off-diagonal subplot. When two parameters are highly correlated, then their estimated values lie on a curve in the scatter plot. This was the case for (τ_0, ν) (first row second plot, second row first plot), but for none of the other groups. For each parameter quartet we plotted the coordinate pair (τ_0, ν) as a colored dot in Figure 5b and calculated the associated G' and G'' to be displayed as gray curves in Figure 5c.

One way to visualize the relationship among the parameters is through a *residual heat map*, as seen for τ_0 and η_p in Figure 5b. For each (τ_0, η_p) pair in the displayed region, we found the combination of N and ν that minimized the residual function (76) and displayed the (τ_0, η_p)-minimal residual value in terms of colors ranging from blue (smallest residual) to yellow (relatively large residual). The presence of the blue-green "residual trough" indicates a region of (τ_0, η_p) that can provide similarly effective fits. Each white dot corresponds to a (N, η_p, τ_0, ν) combination that provided an optimal fit to a randomly perturbed version of the true $\widetilde{G}_r(s)$. The red dot is the parameter combination corresponding to the minimal point in Figure 5a. We emphasize that the trough does indeed tend to capture the manner in which an error in one parameter will be compensated by a specific error in another parameter.

The essential observation in this numerical experiment is demonstrated in Figure 5c. Despite practical unidentifiability among the parameters, the inferred storage and loss moduli are quite consistent for a certain range of frequency ω. In the panel, we have the true $G'(\omega)$ and $G''(\omega)$ in black and overlay in gray the 100 $G'(\omega)$ and $G''(\omega)$

curves each corresponding to one of the parameter combinations associated with the white dots in Figure 5b. There is essentially no variation in the storage modulus G' near the nonmonotonic region which appears in the range $\omega \in (10^2, 10^4)\,\mathrm{s}^{-1}$. We note that this nonmonotonic feature was studied in the single mode case by Marvin and Oser [26, 34], but we do not know of any analysis that exists when there are more Maxwell elements.

3.3.1. Methodology for identifiability analysis. To explain our approach to generating Figures 5b and 5c, we recall from (16) that $\widetilde{G}_r(s) = \eta_s + \frac{\eta_p}{\|K^+\|_1}\widetilde{K}^+(s)$. When $K \in \mathscr{K}_{\mathrm{Rouse}}$, this takes the form

$$\widetilde{G}_r(s) = \eta_s + \frac{\eta_p}{\langle \tau_n \rangle}\frac{1}{N}\sum_{n=1}^{N}\frac{1}{s\tau_0 N^\nu + n^\nu}. \tag{75}$$

We generated 100 sets of T_N target pairs $(s_i, \tilde{g}_i)$, $i \in \{1, 2, \ldots, T_N\}$. Each s_i is the inverse of a data observation time point t_i. We set the corresponding $\tilde{g}_i$ value to be $\tilde{g}_i := \widetilde{G}_r(s_i) + (0.1\widetilde{G}_r(s_i))^{1/2}\epsilon_i$, where ϵ_i is a standard normal random variable.

We then obtained a joint estimate for (η_p, N, τ_0, ν) by computing a solution to the least square fitting problem given by (75), assuming that η_s is known a priori. To be precise, for each N in a reasonable range, we numerically computed the parameter triplet (η_p, τ_0, ν) that minimized the residual function

$$R_N(\{\tilde{g}_i\}\,;\,\eta_p, \tau_0, \nu) := \sum_i \frac{\left(\tilde{g}_i - \widetilde{G}_r(s_i\,;\,N, \eta_p, \tau_0, \nu)\right)^2}{\tilde{g}_i^2}. \tag{76}$$

In practice, this was accomplished using the least square nonlinear fit command in MATLAB. The optimization is constrained below by $\eta_p, \tau_0 \geq 0$, and $\nu \geq 1$. For the numerical experiment associated with Figure 5, we set the true parameters to be $N = 100$, $\eta_s = 10^{-2}\mathrm{g}/(\mathrm{cm\ s})$ corresponding to water, $\eta_p/\tau_{\mathrm{avg}} = 10^3\mathrm{g}/(\mathrm{cm\ s}^2)$ corresponding to $\eta_p \approx 163.5\mathrm{g}/(\mathrm{cm\ s})$, $\tau_0 = 10^{-3}\mathrm{s}$, and $\nu = 2$.

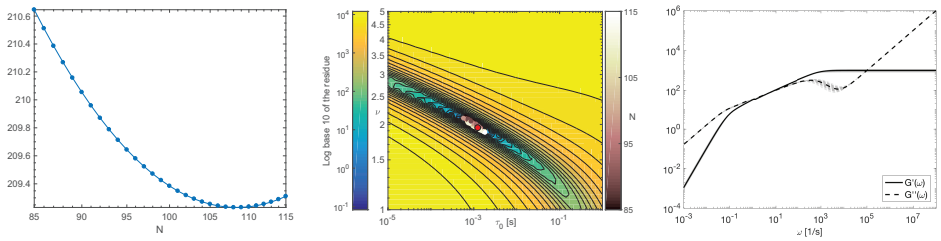

(a) Profile Likelihood for N (b) Residual Surface Plot (c) Storage and Loss Moduli

FIG. 5. Generalized Rouse Spectrum: uncertainty due to $\widetilde{G}_r(s) \longleftrightarrow G^*(\omega)$. *For a fixed parameter set, the corresponding function* $\widetilde{G}_r(s)$ *was perturbed* 100 *times and converted to* $G'(\omega)$ *and* $G''(\omega)$ *according to the procedure described in section* 3.3. *In the* left panel, *a profile likelihood is provided for* N *for one of the* 100 *perturbations. In the* middle panel, *for each* (τ_0, ν) *pair, the color corresponds to the minimum possible residual from the true* $\widetilde{G}_r(s)$ *among all admissible values for* N *and* η_p. *Each white dot corresponds to a parameter combination inferred for one perturbation of the true* $\widetilde{G}_r(s)$. *These collect in a "trough" of the residual map. In the* right panel, *we see* G' *and* G'' *computed for all* 100 *of the perturbations. (*$N = 100$, $\tau_0 = 10^{-3}s$, $\eta_s = 10^{-2}g/(cm\ s)$, $\eta_p/\tau_{avg} = 10^3 g/(cm\ s^2)$.*)*

For notational efficiency, we will suppress dependence on the g_i and write

$$R_N^{\min}(\eta_p, \tau_0, \nu) := \min_{(\eta_p,\tau_0,\nu)} R_N(\{\tilde{g}_i\}\,;\, \eta_p, \tau_0, \nu). \tag{77}$$

It is important to observe that an error in the estimate of one parameter can be "compensated for" by a correlated error in the estimate of another parameter. One way to demonstrate this is through a *profile likelihood* plot, as in Figure 5a. For one instance of a perturbed set of target points $\{s_i, \tilde{g}_i\}$, we plotted $\log_{10} R_N^{\min}(\eta_p, \tau_0, \nu)$ as a function of $N \in \{85, \ldots, 115\}$. We observe that there is a minimum point at $N \approx 107$ indicating that N can be reasonably estimated. However, the $\log_{10}$-residues vary only over a range of two units (from 209.4 to 210.6).

3.4. $[M(t) \longleftrightarrow \widetilde{G}_r(s)]$ converting time domain information to the frequency domain. While the work in the previous section demonstrates identifiability issues that are intrinsic to the Generalized Rouse model for viscoelastic diffusion, a larger source of uncertainty lies in the conversion of path data to a quantity on which one can find optimal paramter sets, i.e., the connection $M(t) \longleftrightarrow \widetilde{G}_r(s)$. As we have described above, Mason and Weitz were the first among many others who chose to compute a numerical Laplace transform of the MSD and use (25) to create an approximation of $\widetilde{G}_r(s)$ on which to perform inference. In principle, one could perform the parameter optimization directly on the MSD. In Lemma 3.3 we provide a formula for the MSD in terms of $\widehat{\rho}(\omega)$. For each parameter combination, it is trivial to compute $\widehat{\rho}(\omega)$; however, we found that in practice, the numerical computation of (78) is subject to extremely large numerical error. Some discussion concerning the computation of such an integral is provided in [15, 14, 13].

LEMMA 3.3. *Let $\{(X(t), V(t))\}_{t\geq 0}$ be defined as in Theorem 2.4. Then*

$$M(t) = \frac{4}{\pi}\int_0^\infty \sin^2\left(\frac{t\omega}{2}\right)\frac{\widehat{\rho}(\omega)}{\omega^2}d\omega. \tag{78}$$

Proof. Recalling that $\rho(t) = \mathbb{E}(V(t)V(0))$ and using the definition of $M(t)$, we have $M(t) = \int_0^t \int_0^t \rho(s - s')ds'ds$. Next, expressing $\rho(s - s')$ in terms of its Fourier inverse transform gives

$$M(t) = \int_0^t \int_0^t \frac{1}{2\pi}\int_{-\infty}^\infty e^{-i(s-s')\omega}\hat{\rho}(\omega)d\omega ds'ds. \tag{79}$$

The claim follows by switching the order of integration in (79), integrating, and using the Euler formula and the fact that $\hat{\rho}(\omega)$ is even. ∎

Computing a numerical Laplace transform presents its own problems. The first, and most prominent, is that because the MSD of a particle is an increasing function, the tail of the integrand of the Laplace transform is not trivial. As is also pointed out in Evans et al. [6], it is necessary to project behavior of the MSD for regions outside of the values given by the data. We suppose the observations are taken over a time interval $t \in [t_1, T]$ which is divided into equally spaced subintervals with observations at the times $t_i := i\Delta t$, $i = 1, \ldots, N_T$. For each i, we write $M_i := M(t_i)$.

It is natural to split the Laplace transform into three regions:

$$\begin{aligned}\widetilde{M}(s) &= I_1(s) + I_2(s) + I_3(s)\\ &:= \int_0^{t_1} e^{-st}M(t)dt + \int_{t_1}^T e^{-st}M(t)dt + \int_T^\infty e^{-st}M(t)dt.\end{aligned} \tag{80}$$

To approximate $I_2(s)$ it is sufficient to use the trapezoidal rule:

$$\int_{t_1}^{T} e^{-st} M(t)dt \approx \widetilde{M}_{\text{trap}}(s) = \frac{\Delta t}{2} \sum_{j=1}^{N_T-1} (e^{-st_{j+1}} M(t_{j+1}) + e^{-st_j} M(t_j)). \tag{81}$$

On the intervals $[0, t_1]$ and $[T, \infty)$, we approximate $M(t)$ by $C_0 t^{q_0}$ and by $C_\infty t^{q_\infty}$, respectively, where the coefficients and exponents are obtained by linearly fitting a small number of points on the beginning and on the tail of $\ln M(t)$ to $\ln t$. In practice, we assume that there are 2048 time points for which the particle position is observed. The ensemble pathwise MSD is very noisy for large time, so it is standard practice to only use the first 10% to 20% of the time points. We therefore set the number of target points to be $N_T = 200$ to find the coefficients.

Outside of the observed range, the approximations simplify to

$$\begin{aligned} \int_0^{t_1} e^{-st} M(t)dt &\approx \frac{C_0}{s^{q_0+1}} \gamma(st_1, q_0 + 1) \text{ and} \\ \int_T^{\infty} e^{-st} M(t)dt &\approx \frac{C_\infty}{s^{q_\infty+1}} \Gamma(sT, q_\infty + 1), \end{aligned} \tag{82}$$

where $\gamma(a, x) = \int_0^x t^{a-1} e^{-t} dt$ is the lower incomplete gamma function and $\Gamma(a, x) = \int_a^\infty t^{a-1} e^{-t} dt$ is the upper incomplete gamma function. Combining (80)–(82), we have

$$\widetilde{M}(s) \approx \widetilde{M}_{\text{app}}(s) = \frac{C_0}{s^{q_0+1}} \gamma(st_1, q_0 + 1) + \widetilde{M}_{\text{trap}}(s) + \frac{C_\infty}{s^{q_\infty+1}} \Gamma(sT, q_\infty + 1). \tag{83}$$

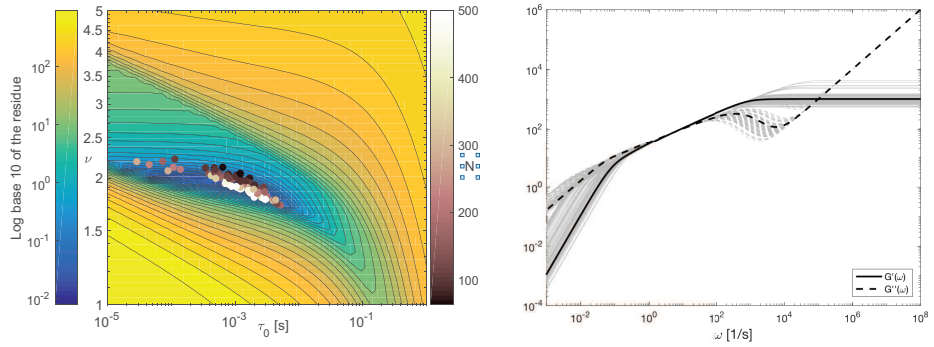

(a) Residual Surface Plot (b) Storage and Loss Moduli

FIG. 6. Monte Carlo visualization of the full method: $\mathcal{M}(t) \longleftrightarrow M(t) \longleftrightarrow \widetilde{G}_r(s) \longleftrightarrow G^*(\omega)$. *For the same baseline parameter set used for Figure 5, we assess uncertainty that arises due to computing an ensemble MSD from simulated data, converting this estimate for the true MSD to an estimate for* $\widetilde{G}_r(s)$ *and finding an optimal parameter fit. In the* left panel*, the location of each dot corresponds to the* (τ_0, ν) *values for each* (τ_0, ν) *pair; the color corresponds to the minimum possible residual from the true* $\widetilde{G}_r(s)$ *among all admissible values for* N *and* η_p*. In the* right panel*, we see* G' *and* G'' *computed for all* 100 (τ_0, ν) *pairs displayed in the middle panel.*

In order to visualize the increased uncertainty that arises from (1) only being able to observe the MSD at a small number of time points, and (2) needing to compute a numerical Laplace transform, we generated a second residual heat map (Figure 6a).

For the given set of 200 time points $\{t_1, t_2, \ldots, T\}$ we generated an associated set of target points $(s_i, \tilde{g}_i)$. For each $i \in \{1, \ldots, N_T\}$, we set $s_i = t_i^{-1}$ and then used (83) to compute $\widetilde{M}_{\rm app}(s_i)$. Then the corresponding estimate $\tilde{g}_i$ for $\widetilde{G}_r(s_i)$ was computed by way of (25) in Theorem 2.4:

$$\tilde{g}_i := \frac{1}{6\pi a}\left[\frac{2c}{s_i^2 \widetilde{M}_{\rm app}(s_i)} - m s_i\right]. \tag{84}$$

As with Figure 5b, the color coding reveals which combinations of τ_0 and ν can be combined with optimal values of N and η_p to yield a function $\widetilde{G}_r(s\,;\, N, \eta_p, \tau_0, \nu)$ that is close to the target values at the frequencies $\{s_i\}$. However, for Figure 6a (and Figure 7a) we introduced a weighted residual function. The reason for the weights is that every $\tilde{g}_i$ value has a contribution from each of $I_1(s_j)$, $I_2(s_j)$, and $I_3(s_j)$ in (80). Importantly, points nearer the boundary of the observation window have larger contributions from I_1 and I_3 which contain the projected information. Moreover, there is reasonable disagreement concerning what is an appropriate projection into the large-t region ($t > T$). As demonstrated by Theorem 2.3, when there are finitely many terms in the Prony series, the sublinear character of the MSD only exists over a finite range. So, eventually the MSD will grow linearly. The question is whether the linear regime will emerge shortly after the observable time range, whether the present power law behavior near time $t = T$ will persist. We have chosen to project the sublinear behavior to all $t > T$, and this is the choice effectively made by the methods adopted by Mason [28] and Dasgupta et al. [4]. However, Evans et al. [6] opted to project into the large-t region with linear growth.

The residuals used in this section are therefore computed with the weights $w_i := I_2(s_i)/\widetilde{M}(s_i)$. In this way, w_i is the fraction of the value $\tilde{g}_i$ that is given by non-projected data points. Then

$$R_N(\eta_p, \tau_0, \nu; w) := \sum_{i=1}^{N_T} w_i^2 \frac{(\tilde{g}_i - \widetilde{G}_r(s_i))^2}{\tilde{g}_i^2}. \tag{85}$$

Note that, as a result of the relatively small number of observed time points and the numerical computation of the Laplace transform, the blue trough of (τ_0, ν) pairs that can be part of "good-fitting quartets" (N, τ_0, ν, η_p) is much larger. As we discuss in the next section, this trough structure captures the shape of the best fit parameter sets for simulated data.

3.5. $[\boldsymbol{\mathcal{M}(t) \longleftrightarrow M(t) \longleftrightarrow \widetilde{G}_r(s) \longleftrightarrow G^*(\omega)}]$ Monte Carlo visualization of uncertainty in the relaxation moduli. We use numerical simulation to portray our final assessment of uncertainty: the *passive microrheology* procedure. Using a covariance-based algorithm to generate GLE paths (described in [13, 15, 14]), we mimic experimental conditions, taking $\Delta t = 2^{-2}$s, $N_T = 2048$, and $N_P = 75$ (number of paths). To construct $\mathcal{M}(t)$, for each path we computed a pathwise MSD, defined as in (11). Then our estimate of the MSD, $M(t)$ was the ensemble average of pathwise MSDs. For our observation times, we chose $t_i = i\Delta t$ for $i \in \{1, \ldots, 200\}$. Given this collection of MSD estimates, we computed the target points $(s_i, \tilde{g}_i)$ as described in the previous section and found the parameter set that minimized the weighted residual function 85.

Each dot in Figure 6a corresponds to a (τ_0, ν) pair that produced an optimal fit for a given path. The color of each dot indicates the associated value of N in the optimal

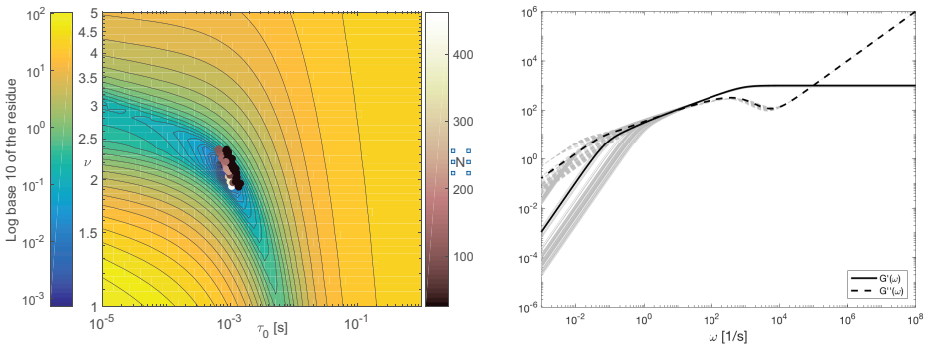

(a) Residual Surface Plot (b) Storage and Loss Moduli

FIG. 7. Assessing the effect of a 100x faster frame rate. *For the same baseline parameter set used in the previous figures, we repeat the procedure applied to create Figure* 6*, but shifted the observation times down by a factor of* 100*. We see that the parameter* τ_0 *can be much better estimated; however, there is greater uncertainty regarding* ν *and* N*. (Uncertainty for* N *not pictured.)*

quartet. From the figure, we see that the estimates for N and τ_0 in particular are quite noisy. However, despite this uncertainty in parameter estimation, the inference for a certain range of the storage and loss moduli is very tight. Indeed, in Figure 6b the gray curves represent the Storage (G', solid) and Loss (G'', loss) moduli associated with each parameter quartet fit.

In Figure 7, we carried out the same procedure for the same parameter set, but then supposed that the experimental camera frame rate is 100 times as fast (but we assume that the movies have the same number of total frames, so we lose observations for larger t). It is interesting to see the change in shape of the blue residual trough. The improved frame rate allows the parametrization to "rule out" the range of τ_0 values $[2 \times 10^{-3}s, 10^{-1}s]$, which were plausible before. Because the range of τ_0 is narrowed, the range of N values is diminished as well. For the storage and loss moduli, the range of ω-values that have good certainty have shifted right, as expected, including the Oser and Marvin feature. In fact, because the estimate for η_p improved considerably, the range of certainty extends well beyond the experimental time scale in the high frequency range.

4. Discussion. Biological fluids, like mucus and the cytoplasm of cells, exhibit a wide range of viscoelastic properties that are essentially impossible to study by traditional rheological techniques. Because fluid samples are intrinsically small and difficult to collect, *micro*rheological tools, which rely on studying the fluctuating behavior of immersed microparticles, have become indispensible. The fundamental challenge for these inference methods though is that while the data is collected in the time domain, the standard characterizations of viscoelastic fluids are articulated in Fourier frequency space. In this work, we have put the fundamental assumptions of what is sometimes called the Mason and Weitz protocol on rigorous footing and attempted to quantify the uncertainty that is introduced in each step of the procedure.

According to the Mason and Weitz hypothesis, the behavior of a particle immersed in a complex fluid is well described by the Generalized Langevin Equation that has a memory kernel that matches the fluid's shear relaxation modulus $G_r(t)$. We accepted this premise as true throughout this work and focused on the problem of inferring the

Laplace transform of $G_r(t)$ from particle position data, which can then be related to $G'(\omega)$ and $G''(\omega)$ by analytic continuation. Mason and Weitz proposed a relationship between a particle's Mean-Squared Displacement and its memory kernel (see (25)), but to the best of our knowledge this formula had never been established rigorously before for stationary solutions of the GLE (Theorem 2.4).

After exploring various representations of the GLE and the Mason and Weitz formula, we proceeded to analyze the inversion procedure itself, reconstructing $G'(\omega)$ and $G''(\omega)$ from particle path data. There have been attempts to do this with a nonparametric approach, but as we argue in section 3.4, and as has been observed elsewhere [6], any procedure that involves numerically relating Mean-Squared Displacement (MSD) of the position process to the Autocovariance Function of the velocity process will require projecting MSD values beyond the experimentally observed time range. By way of the small- and large-ω asymptotics for $G'(\omega)$ and $G''(\omega)$ that we studied in section 3.1, we can argue that the MSD projection will dominate both ω extremes. In other words, the inferred $G'(\omega)$ and $G''(\omega)$ for small- and large-ω will depend more on the projection technique than the actual process, which contradicts the point of using a nonparametric method in the first place. We therefore adopted a form for $G_r(t)$, given in (18), that is well established in polymer physics literature [7]. Moreover, we used a tunable four-parameter family of functions (2.1) for which the GLE can mimic a wide array of experimentally observed behavior [30]. We note that there are other methods for parametrizing Prony series kernels to produce similar behavior (see [21, 18], for example); but we reserve for future work an investigation of what happens when one parametric family is used for inference on a GLE generated by another family.

As seen in section 3.4, even when the correct parametric family is used for reconstruction, there is considerable error introduced by (1) the constraint of finite time series observations, and (2) the conversion time domain information to Fourier frequency space. The error is not uniform in ω though. While we were reluctant to use the precise language of confidence intervals and hypothesis testing (because there are some ambiguities in how such statistical tests should be set up), we introduced a Monte Carlo visualization of the uncertainty intrinsic to passive microrheology. We have showed that, while there can be significant uncertainty in the estimation of certain parameters (in particular, the smallest relaxation time τ_0 and the number of distinct linear relaxation times N (Figures 5b, 6a, and 7a)), there is remarkable consistency in the inferred values for $G'(\omega)$ and $G''(\omega)$ over the range of frequencies that correspond to experimentally observed times (Figures 5c, 6b, and 7b).

This observation is very much in the spirit of many Uncertainty Quantification investigations that show that parameter estimation should not be an end in and of itself. Often, parameter values are useful only to the extent that they help produce some scientifically relevant prediction. When a methodology is sound, as the protocol used for passive microrheology seems to be, the prediction of interest (in our case, characterization of the storage and loss moduli) is robust and stable despite the potential for large error in parameter estimation.

Acknowledgments. The authors thank Hung Nguyen, Gustavo Didier, and Marisa Eisenberg for fruitful conversations in the development of this work.

REFERENCES

[1] F. Baudoin, *Diffusion Processes and Stochastic Calculus*, European Mathematical Society/American Mathematica, Zürich, 2014.

[2] D. Chen, A. Lau, L. Hough, M. Islam, M. Goulian, T. Lubensky, and A. Yodh, *Fluctuations and rheology in active bacterial suspensions*, Phys. Rev. Lett., 99 (2007), 148302.

[3] J. Crocker, M. Valentine, E. Weeks, T. Gisler, P. Kaplan, A. Yodh, and D. Weitz, *Two-point microrheology of inhomogeneous soft materials*, Phys. Rev. Lett., 85 (2000), pp. 888–891.

[4] B. R. Dasgupta, S.-Y. Tee, J. C. Crocker, B. J. Frisken, and D. A. Weitz, *Microrheology of polyethylene oxide using diffusing wave spectroscopy and single scattering*, Phys. Rev. E, 65 (2002), 051505.

[5] M. C. Eisenberg, S. L. Robertson, and J. H. Tien, *Identifiability and estimation of multiple transmission pathways in cholera and waterborne disease*, J. Theor. Biol., 324 (2013), pp. 84–102.

[6] R. Evans, M. Tassieri, D. Auhl, and T. A. Waigh, *Direct conversion of rheological compliance measurements into storage and loss moduli*, Phys. Rev. E, 80 (2009), 012501.

[7] J. D. Ferry, *Viscoelastic Properties of Polymers*, John Wiley & Sons, New York, 1980.

[8] J. Fricks, L. Yao, T. C. Elston, and M. G. Forest, *Time-domain methods for diffusive transport in soft matter*, SIAM J. Appl. Math., 69 (2009), pp. 1277–1308, https://doi.org/10.1137/070695186.

[9] I. Goychuk, *Viscoelastic subdiffusion: From anomalous to normal*, Phys. Rev. E, 80 (2009), 046125.

[10] I. Goychuk, *Viscoelastic subdiffusion: Generalized langevin equation approach*, Adv. Chem. Phys., 150 (2012), pp. 187–249.

[11] M. Grimm, S. Jeney, and T. Franosch, *Brownian motion in a maxwell fluid*, Soft Matter, 7 (2011), pp. 2076–2084.

[12] D. B. Hill, P. A. Vasquez, J. Mellnik, S. A. McKinley, A. Vose, F. Mu, A. G. Henderson, S. H. Donaldson, N. E. Alexis, R. C. Boucher, and M. G. Forest, *A biophysical basis for mucus solids concentration as a candidate biomarker for airways disease*, PLoS ONE, 9 (2014), e87681.

[13] C. Hohenegger, *On equipartition of energy and integrals of Generalized Langevin Equations with generalized Rouse kernel*, Commun. Math. Sci., 15 (2017), pp. 539–554.

[14] C. Hohenegger, R. Durr, and D. M. Senter, *Mean first passage time in a thermally fluctuating viscoelastic fluid*, J. Non-Newton. Fluid Mech., 242 (2017), pp. 48–56.

[15] C. Hohenegger and S. A. McKinley, *Fluid-particle dynamics for passive tracers advected by a thermally fluctuating viscoelastic medium*, J. Comput. Phys., 340 (2017), pp. 688–711.

[16] T. Indei, J. D. Schieber, A. Córdoba, and E. Pilyugina, *Treating inertia in passive microbead rheology*, Phys. Rev. E, 85 (2012), 021504.

[17] G. R. Kneller, *Generalized Kubo relations and conditions for anomalous diffusion: Physical insights from a mathematical theorem*, J. Chem. Phys., 134 (2011), 224106.

[18] S. C. Kou, *Stochastic modeling in nanoscale biophysics: Subdiffusion within proteins*, Ann. Appl. Stat., 2 (2008), pp. 501–535.

[19] R. Kubo, *Statistical Mechanics. An Advanced Course with Problems and Solutions*, North-Holland, Amsterdam, 1965.

[20] R. Kubo, *The fluctuation-dissipation theorem*, Rep. Prog. Phys., 29 (1966), pp. 255–284.

[21] R. Kupferman, *Fractional kinetics in Kac–Zwanzig heat bath models*, J. Statist. Phys., 114 (2004), pp. 291–326.

[22] S. K. Lai, Y.-Y. Wang, D. Wirtz, and J. Hanes, *Micro-and macrorheology of mucus*, Adv. Drug Deliv. Rev., 61 (2009), pp. 86–100.

[23] W. Lai, S. Kuei, and V. Mow, *Rheological equations for synovial fluids*, J. Biomech. Eng., 100 (1978), pp. 169–186.

[24] R. G. Larson, *Constitutive Equations for Polymer Melts and Solutions*, Butterworth-Heinemann, Oxford, 1988.

[25] A. J. Levine and T. C. Lubensky, *One-and two-particle microrheology*, Phys. Rev. Lett., 85 (2000), pp. 1774–1777.

[26] R. S. Marvin and H. Oser, *A model for the viscoelastic behavior of rubberlike polymers including entanglements effects*, J. Res. Natl. Bur. Stand. B, 66 (1962), pp. 171–180.

[27] T. Mason and D. Weitz, *Optical measurements of frequency-dependent linear viscoelastic moduli of complex fluids*, Phys. Rev. Lett., 74 (1995), pp. 1250–1253.

[28] T. G. Mason, *Estimating the viscoelastic moduli of complex fluids using the generalized Stokes-Einstein equation*, Rheol. Acta, 39 (2000), pp. 371–378.

[29] G. Massiera, K. M. Van Citters, P. L. Biancaniello, and J. C. Crocker, *Mechanics of single cells: Rheology, time dependence, and fluctuations*, Biophys. J., 93 (2007), pp. 3703–3713.
[30] S. A. McKinley, L. Yao, and M. G. Forest, *Transient anomalous diffusion of tracer particles in soft matter*, J. Rheol., 53 (2009), pp. 1487–1506.
[31] R. Morgado, F. A. Oliveira, G. G. Batrouni, and A. Hansen, *Relation between anomalous and normal diffusion in systems with memory*, Phys. Rev. Lett., 89 (2002), 100601.
[32] H. Mori, *Transport, collective motion, and Brownian motion*, Prog. Theor. Phys., 33 (1965), pp. 423–455.
[33] H. Nguyen and S. A. McKinley, *Anomalous Diffusion and the Generalized Langevin Equation*, preprint, https://arxiv.org/abs/1711.00560, 2017.
[34] H. Oser and R. S. Marvin, *Effect of molecular weight on viscoelastic properties of polymers as predicted by a molecular theory*, J. Res. Nat. Bur. Stand. B, 67 (1963), pp. 87–90.
[35] M. Ottobre and G. Pavliotis, *Asymptotic analysis for the generalized Langevin equation*, Nonlinearity, 24 (2011), pp. 1629–1653.
[36] G. A. Pavliotis, *Stochastic Processes and Applications*, Texts Appl. Math. 60, Springer, New York, 2014.
[37] A. Raue, C. Kreutz, T. Maiwald, J. Bachmann, M. Schilling, U. Klingmüller, and J. Timmer, *Structural and practical identifiability analysis of partially observed dynamical models by exploiting the profile likelihood*, Bioinformatics, 25 (2009), pp. 1923–1929.
[38] F. Reif, *Fundamentals of Statistical and Thermal Physics*, Waveland Press, Nong Grove, IL, 1965.
[39] T. M. Squires and T. G. Mason, *Fluid mechanics of microrheology*, Annu. Rev. Fluid Mech., 42 (2010), pp. 413–438.
[40] L. Starrs and P. Bartlett, *One- and two-point micro-rheology of viscoelastic media*, J. Phys. Condens. Matter, 15 (2003), pp. S251–S256.
[41] M. T. Valentine, Z. E. Perlman, M. L. Gardel, J. H. Shin, P. Matsudaira, T. J. Mitchison, and D. A. Weitz, *Colloid surface chemistry critically affects multiple particle tracking measurements of biomaterials*, Biophys. J., 86 (2004), pp. 4004–4014.
[42] K. Xu, M. Forest, and I. Klapper, *On the correspondence between creeping flows of viscous and viscoelastic fluids*, J. Non-Newton. Fluid Mech., 145 (2007), pp. 150–172.
[43] R. Zwanzig, *Nonlinear generalized Langevin equations*, J. Stat. Phys., 9 (1973), pp. 215–220.
[44] R. Zwanzig and M. Bixon, *Hydrodynamic theory of the velocity correlation function*, Phys. Rev. A, 2 (1970), pp. 2005–2012.